*Report No. UT-03.33*

# *FLEXURAL PERFORMANCE OF DETERIORATED REINFORCED CONCRETE CANTILEVERED BENT CAPS – PART 1*

**By: Fernando Fonseca, Ph.D., P.E.**
**Mark David Rowe**

**Department of Civil & Environmental Engineering**
**Brigham Young University**
**Provo, Utah**

**Utah Department of Transportation**
**Research Division**

**December 2003**

# UDOT RESEARCH & DEVELOPMENT REPORT ABSTRACT

| | | |
|---|---|---|
| **1. Report No.** UT-03.33 | **2. Government Accession No.** | **3. Recipient's Catalog No.** |
| **4. Title and Subtitle**<br>Flexural Performance of Deteriorated Reinforced Concrete Cantilevered Bent Caps – Part 1 | **5. Report Date** December 2003 | |
| | **6. Performing Organization Code** | |
| **7. Author(s)**<br>Fernando Fonseca, Ph.D., P.E.<br>Mark David Rowe | **8. Performing Organization Report No.** | |
| **9. Performing Organization Name and Address**<br>Brigham Young University<br>Department of Civil and Environmental Engineering<br>168 Clyde Building<br>Provo, UT 84604 | **10. Work Unit No.** | |
| | **11. Contract No.** 01-9092 | |
| **12. Sponsoring Agency Name and Address**<br>Utah Department of Transportation<br>Research Division<br>4501 South 2700 West<br>Salt Lake City, Utah | **13. Type of Report and Period Covered** | |
| | **14. Sponsoring Agency Code** | |

**15. Supplementary Notes**
This report complements "Flexural Performance of Retrofitted Reinforced Concrete Cantilevered Bent Caps – Part 2" UT-03.34.


**16. Abstract**

The cantilevered bent caps of four reinforced concrete bridges were tested to determine the effects of deterioration on these bent caps. Two of the bent caps (12S and 12N) were obtained from the demolition of I-15 in Utah. The bent caps were designed in 1963 and built soon thereafter. The other two bent caps (1N and 2N) were new construction and built to the same design specifications as the existing bents. The existing bent caps had suffered varying degrees of deterioration, including significant spalling of the concrete on the underside of the cantilever and corrosion of the stirrups. Several stirrups in each bent caps were corroded completely through on the underside of the cantilever. The bent caps 12S and 1N were tested to failure. The other two bent caps, 12N and 2N, were tested to their approximate yield point. Strain gauges were mounted on the concrete surface on the sides of the bent. Strain gauges were also mounted on the reinforcement of the two new bent caps constructed. Strain distributions were approximately linear at measured locations. Bent cap 12S yielded at a load of 625 kips [2,781 kN], corresponding to a displacement of 0.78 in [20 mm], and had a peak load of 709 kips [3,155 kN]. Bent cap 12N was loaded to 560 kips [2,492 kN] and displayed a linear load–displacement relationship to that point. Bent cap 1N yielded at 587 kips [2,612 kN], corresponding to a displacement of 0.90 in. [23 mm], and had a peak load of 708 kips [3,151kN]. Bent cap 2N was loaded to 560 kips [2,492kN] and also displayed a linear load–displacement relationship to that point. Predicted capacities for the bent caps were calculated using the 1963 AASHO code (Working Stress Design), 1996 AASHTO code (Ultimate Strength Design), and Strut and Tie models. Both Working Stress Design and Ultimate Strength Design assume Bernoulli beam theory, which best approximated the capacity of the bent caps. The conclusion from the tests conducted and the calculations of predicted capacity is that the deterioration did not affect the strength of the existing bent caps.


| | | | |
|---|---|---|---|
| **17. Key Words** | | **18. Distribution Statement**<br>Available: UDOT Research Division<br>P.O. Box 148410<br>Salt Lake City, UT 84114-8410<br>www.udot.utah.gov | |
| **19. Security Classification (of this report)**<br>N/A | **20. Security Classification (of this page)**<br>N/A | **21. No. of Pages**<br>94 | **22. Price** |

THIS PAGE LEFT BLANK INTENTIONALLY

# EXECUTIVE SUMMARY

The cantilevered bent caps of four reinforced concrete bridges were tested to determine the effects of deterioration on these bent caps. Two of the bent caps (12S and 12N) were obtained from the demolition of I-15 in Utah. The bent caps were designed in 1963 and built soon thereafter. The other two bent caps (1N and 2N) were new construction and built to the same design specifications as the existing bents.

The existing bent caps had suffered varying degrees of deterioration, including significant spalling of the concrete on the underside of the cantilever and corrosion of the stirrups. Several stirrups in each bent caps were corroded completely through on the underside of the cantilever.

The bent caps 12S and 1N were tested to failure. The other two bent caps, 12N and 2N, were tested to their approximate yield point. Strain gauges were mounted on the concrete surface on the sides of the bent. Strain gauges were also mounted on the reinforcement of the two new bent caps constructed. Strain distributions were approximately linear at measured locations.

Bent cap 12S yielded at a load of 625 kips [2,781 kN], corresponding to a displacement of 0.78 in [20 mm], and had a peak load of 709 kips [3,155 kN]. Bent cap 12N was loaded to 560 kips [2,492 kN] and displayed a linear load–displacement relationship to that point. Bent cap 1N yielded at 587 kips [2,612 kN], corresponding to a displacement of 0.90 in. [23 mm], and had a peak load of 708 kips [3,151kN]. Bent cap 2N was loaded to 560 kips [2,492kN] and also displayed a linear load–displacement relationship to that point.

Predicted capacities for the bent caps were calculated using the 1963 AASHO code (Working Stress Design), 1996 AASHTO code (Ultimate Strength Design), and Strut and Tie models. Both Working Stress Design and Ultimate Strength Design assume Bernoulli beam theory, which best approximated the capacity of the bent caps.

The conclusion from the tests conducted and the calculations of predicted capacity is that the deterioration did not affect the strength of the existing bent caps.

THIS PAGE LEFT BLANK INTENTIONALLY

TABLE OF CONTENTS

Page

# ACKNOWLEDGEMENTS

The authors would like to thank the financial support given by the Utah Department of Transportation and the tremendous assistance of Bruce and Chris from Restruction Corp. Gerber Construction and Elitecrete are also acknowledged for their work and cooperation.

LIST OF TABLES

LIST OF FIGURES

THIS PAGE LEFT BLANK INTENTIONALLY

# 1. Introduction

## 1.1 Scope of Work

The cantilevered bent caps of four reinforced concrete bridges were tested to determine the effects of deterioration on these bent caps, know hereafter as *bent*. Two of the bents tested were designed and built in the 1960's. The other two bents were new construction and built to the same specifications as the existing bents. Two bents were tested to failure — one existing and one new. The other two bents were tested to their approximate yield point. The response and behavior of the bents were compared to determine if deterioration significantly affects the strength and performance of the bents.

The existing bents were obtained from the 6$^{th}$ South viaduct in Salt Lake City, Utah. During the summer of 1999, the viaduct was torn down and replaced as part of the I-15 reconstruction. This viaduct was designed and built during the early 1960's. Figures 1.1 and 1.2 show the three bents and the cantilever portion of one of the bents, respectively. Figures 1.3 – 1.7 show the condition of the existing bents prior to testing. As seen in these figures, the bents had suffered varying degrees of deterioration and corrosion due to the exposure to deicing salts and almost 40 years of freeze-thaw cycles.

## 1.2 Influence of Span to Depth Ratio on the Capacity of Beams

The response of the bents considered in this research may not be governed by a flexure beam theory due to their small span to depth ratio. The American Concrete Institute (ACI, 1999) code specifies that deep beam action must be considered when the clear span to depth ratio of a beam is less than 2.5 for continuous spans or 1.25 for simple spans. The clear span to depth ratio of the bents considered in this research, however, is difficult to determine because of the varying depth of the bent. A review of the literature related to the response of beams with small span to depth ratio was therefore conducted to determine its applicability to the bents tested under this research initiative. Unfortunately, the number of publications discussing the response of beams with small span to depth ratio is relative small. Thus, a synopsis of the two most relevant testing programs to determine the capacity and to understand the behavior of beams with small span to depth ratio is presented in this section.

Rogowsky et al. (1986a) tested several reinforced concrete deep beams. The shear span to effective height (a/d) ratio and vertical and horizontal shear reinforcement

were varied. Concrete strengths were low-to-medium varying from 2000 psi (26.1 Mpa) to 6800 psi (46.8 Mpa). Beams with little or no vertical shear reinforcement showed evidence of tied-arch action due to the almost constant strain in the tension steel from one end of the beams to the other. Beams with high vertical shear reinforcement, however, did not have constant strain in the tension steel, rather strain diagrams that were similar to moment diagrams. Failure of these highly shear reinforced beams exhibited a high degree of ductility ultimately failing by the crushing of the top of the compression zone. Two main conclusions were made from that study: (a) beams without stirrups or with minimum stirrups behaved as a tied-arch at failure regardless of the amount of horizontal web reinforcement, and (b) beams with large amounts of stirrups failed in a ductile manner. Furthermore, measured capacity for simple beams compared well with those predicted by the empirically based ACI code equations whereas the continuous beam capacities were not well predicted.

More recently, Tan et al., (1997) tested also several reinforced concrete deep beams. The main variables of testing program were the concrete strength, which exceeded 8000 psi (55 Mpa); the shear span to overall height (a/h) ratios, which ranged from 0.25 to 2.5; and main steel ratio, which varied from 2.00 to 5.80 percent. The purpose of the testing program was to determine the influence of the reinforcement and shear span to overall height ratios on the shear response of high strength concrete deep and short beams. The conclusions from that testing program were (a) the transition between high strength concrete deep beams and high strength concrete shallow beams occurs approximately at shear span to overall height ratios of 1.5, which is slightly different that that for low-to-medium strength concrete beams; (b) the failure mode is influenced mainly by the a/h ratios — for $a/h = 0.25$ beams fail in bearing, for $0.25 < a/h = 1.00$ beams fail in shear-compression, for $1.00 < a/h = 2.00$ beams fail in diagonal tension, and for $a/h = 2.50$ beams fail in shear-tension; (c) increasing the reinforcement ratio will increase the load capacity of beams with $a/h = 1.50$; (d) the ACI code is conservative for predictions of cracking strengths of high strength concrete deep and short beams with reinforcement ratio between 1.23 to 5.80 percent; (e) and the ACI code is non conservative when a/h of high strength concrete beams exceeds 1.50.

Based on the literature reviewed, the response of the bents to be tested in this experimental program may differ from that of slender beams due to their span to depth ratio.

### 1.3 Analysis and Design of Beams with Small Span to Depth Ratio

Similar to slender beams, beams with small span to depth ratio must be designed for flexure as well as for shear. The ACI code specifies that deep flexural members, in other words beams whose depth is large when compared to their length, must be designed for flexure by taking into account the nonlinear distribution of strain. No specific guidelines, however, are given on how to accomplish such a task. Suggestions for the design of deep beams for flexure are given in a publication by the Portland Cement Association (1946) and in the work of Chow et al. (1953), and Park and Paulay (1975). A review of these references is beyond the scope of this report. Unlike for flexure, the ACI code has special provisions for the shear design of deep flexural members. Those provisions as well as the provisions for shear design of slender flexural members are based on the results of more than 250 tests on beams of both small and large span to depth ratios. The results of these tests are reported in ACI-ASCE Committee 426 (1973), ACI-ASCE Committee 426 (1974), dePaiva and Siess (1965), and Crist (1966). A review of these references is also beyond the scope of this report.

There are three main approaches to analyze and design deep flexural members for shear: empirical methods, stress-strain analysis, and mechanics based models. As mentioned above, current design codes are empirical based. A stress-strain analysis, although not commonly conducted is allowed by design codes. A two or three dimensional analysis, either linear or non linear can be easily accomplished using structural software. Mechanics based model are simple to develop and reasonably accurate. In one such model, the strut and tie model, the member is idealized as a series of tension ties, concrete struts, load, and supports interconnected at nodes to form a truss (Rogowski and MacGregor, 1986b). In fact, many researchers are proponents of the strut and tie model for the shear design of deep flexural members instead of the empirically based ACI Code equations because of inaccuracies (Rogowsky et al., 1986a). The use of the strut and tie model to idealize deep flexural members is briefly presented in the remaining of this section while a theoretical explanation of the model is given in Section 2.

Marti (1985) was one of the first proponents of the strut and tie model for concrete design because of its simplicity and adaptability to various geometries. The model was defined as discrete images of statically equivalent stress fields. For struts

and nodal zones, the author suggested an average value of 0.6 times the compressive strength of the concrete ($f'_c$) to estimate the effective concrete strength.

Rogowsky and MacGregor (1986b) compared the capacity of several deep beams with the capacity predicted by strut and tie models. The main conclusion was that strut and tie models give good agreement with tests results. The authors, however, cautioned users that an appropriate truss model is one which correctly identifies the reinforcement which is at yield at failure and discounts the remaining reinforcement.

Kesner and Poston (2000) discussed using the strut and tie model for the purpose of analyzing existing structures. Five steps were presented for analyzing deep beams with the strut and tie model: (1) determine the boundaries regions with a nonlinear strain profile and the forces along these boundaries; (2) develop a truss model within the boundaries that takes into consideration the location of reinforcement and dimensions of the concrete struts; (3) conduct an analysis to determine the forces in each of the strut and tie in the model; (4) determine the capacity of the system from the forces in each member; and (5) detail the regions where struts and ties meet and the tension reinforcement is necessary to enable the model to fully develop. The authors pointed out the main advantages of using the strut and tie model over more traditional methods: simple modeling of the mechanics of the structure, ease identification of critical sections for development of reinforcement, and flexibility to adapt to unusual geometries.

Rogowsky and MacGregor (1986b) provided four suggestions for the development of an efficient and accurate strut and tie model: (1) use strut angles between 25 and 65 degrees; (2) use a strut efficiency factor of 0.6; (3) provide stirrups that have a capacity of at least 30% of the shear force in the beam; and (4) consider support settlements for continuous beams.

Based on the existing research, strut and tie models are simple to develop and accurate. Thus, the bents considered in the present testing program will be analyzed using methods based on flexure beam theories as the mechanics based strut and tie model.

# 2. Design Capacities

As discussed in section 1, the response of the bents considered in this research may or may not be governed by a flexure beam theory due to their small span to depth ratio. Thus, methods based on Bernoully beam theory as well as mechanics based models will be used to calculate the capacity of the bents. Such an analysis is necessary to determine expected force and displacement magnitudes during testing of the bents and to determine which approach will better predict the capacity of the bents.

The shear capacity and flexural capacity of the bents were estimated using four different procedures: Working Stress Design, Ultimate Strength Design, Moment Curvature, and Strut and Tie Modeling. In the analyses conducted the deterioration of the bents was ignored in order to estimate the original design capacity.

## 2.1 Material Properties

The bents were specified to have 3,000 psi (20,670 kPa) concrete and the reinforcement used was grade 40.

Two cores were obtained from one of the bents to determine the compressive strength the concrete. The tests of the cores resulted in an average compression strength of 5,600 psi (38,584 kPa), which was significantly higher than the specified concrete strength.

Tests were also conducted on the reinforcement. The average yield strength was determined to be 43 ksi (296 MPa)

Material tests were conducted after the bents were tested. Preliminary calculations were conducted using specified values. Calculations discussed in this section were revised using actual values.

## 2.2 Bernoulli Beam Theory Methods

### 2.2.1 Working Stress Design

Working Stress Design (WSD) was the method used in 1963, when the bents were designed. Provisions from the American Association of State Highway Officials (1961), known as AASHO (currently known as AASHTO), were used together with the WSD procedure.

The main underlying assumption in WSD is Bernoulli beam theory. The calculations are made by assuming a linear strain profile. Essentially the stress in the reinforcement is multiplied by the area of reinforcement and then by the distance to the centroid of the concrete stress. The result of these multiplications is the maximum allowable moment. The AASHO of 1991 limited the stress in the reinforcement to 20 ksi (138 Mpa). The stress in the concrete was also limited to 0.4 times $f'_c$, where $f'_c$ is the compression strength of the concrete.

In the analysis, the critical section for shear was assumed to be directly next to the loading point and the critical section for flexure was assumed to be at the column face. The capacity of the bent is summarized in Table 2.1. According to the WSD method, the shear capacity is 226 kips (1,006 kN) and the flexural capacity is 1,426 kip-ft (1,934 kN-m). These capacities correspond to concentrated loads of 226 kips (1,006 kN) and 228 kips (1,015 kN), respectively.

### 2.2.2 Ultimate Strength Design

Ultimate Strength Design (USD) is the current standard method. Provisions from the American Association of State Highway and Transportation Officials (1996), known as AASHTO, were used.

Bernoulli beam theory is also the basis for the USD method. The method assumes a linear strain distribution through the depth of the cross section and the reinforcement is allowed to yield. The moment capacity is calculated by multiplying the yield strength of the reinforcement by the area of reinforcement and then by the distance to the centroid of the equivalent concrete stress block.

Similar to the WSD method, the critical section for shear was assumed to be directly next to the loading point and the critical section for flexure was assumed to be at the column face for the USD method. The capacities are summarized in Table 2.1. According to the USD method, the shear capacity of 476 kips (2,118 kN) and the flexural capacity is 3,028 kip-ft (4,105 kN-m). These capacities correspond to concentrated loads of 476 kips (2,118 kN) and 484 kips (2,154 kN), respectively.

### 2.2.3 Moment Curvature

Moment curvature analyses, which are based on Bernoulli beam theory, were also conducted on the bents. Theoretical moment curvature results were obtained from

three sources: BIAX (Wallace and Moehle, 1989), Response (Collins and Mitchell, 1992), and hand calculations. The cross section 6.25 ft (1.9 m) from the tip of the cantilever was used in each of the analyses.

Moment-curvature analyses were conducted using the properties of the material of the new bents. Construction details are discussed on Section 3.

#### 2.2.3.1 BIAX

BIAX was developed at the University of California at Berkeley (Wallace and Moehle, 1989). Bernoulli beam theory and a linear strain profile are assumed in the program. The ultimate strain of concrete was assumed to be 3,000 microstrain and the modulus of rupture of the concrete was assumed to be 493 psi (3,397 kPa). The yield strength of the reinforcement was 61.6 ksi (424 Mpa). A modulus of elasticity of 29,000 ksi (199,000 Mpa) was assumed.

Figure 2.1 shows the moment-curvature for the bent. Concrete cracking is shown by the stiffness occurred at a moment of 812 kip-ft (1,100 kN-m) and a curvature of $6.5 \times 10^{-6}$ rad/in ($2.6 \times 10^{-6}$ rad/cm). Yield occurred at a moment of 2,757 kip-ft (3,738 kN-m) and a curvature of $61 \times 10^{-6}$ rad/in ($24 \times 10^{-6}$ rad/cm).

#### 2.2.3.2 Response

Response accompanies the Prestressed Concrete book (Collins and Mitchell, 1990). Bernoulli beam theory and a linear strain profile are also assumed in the analysis. The assumptions used for the analysis were those made for the BIAX analysis.

Figure 2.1 shows the moment-curvature for the bent. The concrete section cracks at a moment of 859 kip-ft (1,165 kN-m) and a curvature of $6 \times 10^{-6}$ rad/in ($2.4 \times 10^{-6}$ rad/cm). The yield point occurred at a moment of 3,144 kip-ft (4,263 kN-m) and a curvature of $60 \times 10^{-6}$ rad/in ($24 \times 10^{-6}$ rad/cm).

#### 2.2.3.3 Hand Calculations

Hand calculations were also conducted using standard $M_{cr}$ and $M_y$ equations. The curvature was then calculated for the two moments.

Figure 2.1 shows the two calculated values. The concrete cracks at a moment of 716 kip-ft (971 kN-m) and a curvature of $5 \times 10^{-6}$ rad/in ($2.0 \times 10^{-6}$ rad/cm). The section

yields at a moment of 2,514 kip-ft (3,409 kN-m) and a curvature of $54x10^{-6}$ rad/in ($2.1x10^{-6}$ rad/cm).

### 2.2.4 Yield Displacement Calculations

Yield displacements were determined by the Bernoulli beam theory, which neglects shear deformation, and by the Timoshenko beam theory, which includes shear deformation. The standard displacement equations are not valid because the cross section, and therefore the moment of inertia, is not constant. The calculated displacements are shown in Table 2.2. Displacements increased by approximately 0.04 in. (1 mm) when shear deformation was considered.

## 2.3 Mechanics Based Models

Deep beams have been shown to have nonlinear strain distributions through the cross section (MacGregor, 1997). As a result of the nonlinear strain distribution, Bernoulli beam theory does not predict accurate load capacities for deep beams. The regions in the beam where nonlinear strain distributions occur are commonly referred to as D-regions, or disturbed regions. The analysis of D-regions is usually complex unless mechanics based models, such as a truss model, are used to represent the deep beam.

The bents considered in this research may or may not have D-regions due to their small span to depth ratio. The depth of the cross section varies linearly from 36 in. (92 cm) at the tip of the cantilever to 60 in (153 cm) at the column face. The shear span (distance from the loading point to the support) to depth ratio has a value of 1.6, using the bent depth at the column face. Beams with a shear span to effective depth (a/d) ratio between 1.00 and 2.5 are classified as short beams (ACI-ASCE Committee 426). Although the ACI code (1999) provides a definition for deep beams, such a definition is not readily applicable to cantilever beams. A deep beam is defined as a beam with a clear span to depth ratio ($l_n/d$) less than 5. Clear span is the distance between two supports. In the case of a cantilever there is only one support, so the $l_n/d$ ratio is difficult to quantify.

Flexural members, such as the bents considered in this research, may be analyzed and designed by empirical equations or by methods that satisfy equilibrium and strength requirements (ACI, 1999). Therefore, mechanics based models such as the strut and tie model can be used because they always satisfy equilibrium and strength

requirements. Strut and tie models have been shown to estimate accurately the load capacities for D-regions of a deep beam (MacGregor, 1997). Due to its versatility, strut and tie modeling also provides a rational method for analyzing irregular geometric shapes of structural members.

A strut and tie model is a system of forces in equilibrium with a given set of loads. When applied to concrete members, the system of forces has several components. The most basic components of the strut and tie model are ties, struts, and nodes (Rogowsky and MacGregor 1986b). Ties are the tension members, struts are the compression members and nodes are the pins at the joints. When analyzing a reinforced concrete member using a strut and tie model, an equivalent truss is set up using the reinforcement as ties and positioning struts within the concrete dimensions. The equivalent truss must be set up to satisfy equilibrium requirements. The model is assumed to have centerlines of every member coinciding at a point, which implies that there are no moments in the members of the model. The location where the centerlines meet is a node. The strengths of each strut, tie, and node must be checked to ensure that the concrete or reinforcing bar is actually capable of carrying those loads.

The strut and tie model is based on the following assumptions (Rogowsky and MacGregor, 1986a):

1. Equilibrium is satisfied.
2. Concrete has no tensile strength and a compressive strength of $f_{ce} = ?f'_c$ where ? is an efficiency factor, $f_{ce}$ is the effective concrete strength, and $f'_c$ is the specified concrete compressive strength.
3. Reinforcement resists all tensile forces.
4. The centerlines of truss members and external loads are concentrically applied at the nodes.
5. Failure is defined when a concrete strut fails or enough tensile members yield to form a mechanism.

Various methods for determining the efficiency factor exist. The layout of the model, however, is of more importance than finding the correct efficiency factor ( Rogowsky and MacGregor, 1986b).

Two factors aided in the development of the strut and tie model used to analyze the bents: a log of the crack patterns and strain gauge data. The crack pattern provided a visualization of the flow of forces in the bents while strain gauge data provided a

numerical validation of the forces in the model. Both of these factors decreased the number of iterations needed to develop a strut and tie model for the bents.

Several models were developed in an attempt to find one that accurately predicted the yield strength of the bents. Models were developed with varying numbers of stirrups at yield. One of the difficulties in developing an accurate model is determining which reinforcement is at yield and actively involved in the distribution of the forces. The stirrups must be assumed to be at yield to make the truss statically determinate. Because an analysis, as opposed to design, was being conducted, the main flexural reinforcement was assumed to be at yield in all models except No. 6, and the resulting load was determined. The assumption that the main flexural reinforcement yielded was correct as confirmed by the tests results, which will be presented and discussed later.

Table 2.3 shows the matrix of the models developed and the factors in each one. The factors in each model are the number of stirrups at yield, whether or not the main flexural steel is at yield, and the presence of a main compression strut. Model No. 1 is the simplest strut and tie model possible. The main compression strut is shown in Figure 2.2 from the loaded node to the node in the column and the main tension tie from the loaded node to the support. Figure 2.3 shows model No. 3, which is a more typical model. The main difference between the models is the number of active stirrups. All of the models, except model No. 6, assumed that the main flexural reinforcement as well as the stirrups had yielded. This was assumed as a result of the strength of the main compression strut, since the main flexural reinforcement would have yielded before the capacity of the strut was reached.

The forces in the members were determined from the yield strength of the reinforcement bars. Using $F=A_s f_y$, where F is the force in the member, $A_s$ is the area of steel, and $f_y$ is the yield strength of the steel, the stirrups force was calculated to be 49 kips (218 kN) and the top flexural steel yield load to be 655 kips (2915 kN).

### 2.4 Capacity Summary

Table 2.1 summarizes the capacities from the WSD, USD and the moment curvature analyses and Table 2.4 summarizes the capacities of the different strut and tie models. The moment curvature analyses were not conducted at the critical cross section and therefore resulted in higher values for the bent capacity. The USD method predicted the highest capacity of the Bernoulli Beam theory methods. The estimated

capacity being 484 kips (2154 kN). The USD method estimated an ultimate shear capacity of 476 kips (2118 kN).

The difference between the WSD and USD capacities is that WSD is based on allowable stress while USD is based on yield stress. The resulting safety factor of the USD method is just over 2.0. This is due to the limitation in the reinforcement stress which was limited to 20 ksi (138 Mpa) in the WSD method while the yield strength was approximately 43 ksi (296 MPa).

Table 2.4 shows the resulting overall load and main compression strut load from each strut and tie model. The model with the highest load was model No. 2. This model had two stirrups and the main flexural reinforcement at yield and resulted in a point load of 441 kips (1963 kN). The model with the lowest load of 425 kips (1892 kN) was model No. 1. In this model, the main flexural reinforcement was at yield, but no stirrups were at yield.

## 3. Construction of Two New Bents

Two new bents were constructed to compare with the old deteriorated bents. Construction was done according to structural drawings provided by the Utah Department of Transportation (UDOT). Figure 3.1 shows the reinforcement cage for one of the bents. Figure 3.2 shows the forms for one of the bents before the rebar cage was placed inside the forms. Figure 3.3 shows a new bent after the forms had been removed.

The original bents were designed and constructed in the early 1960's when Grade 40 rebar was widely used. Currently, Grade 40 rebar is unavailable. Because of the transition to Grade 60 rebar in the new bents, two options were explored. The first was to decrease the number of bars while maintaining approximately the same area-to-yield-strength ratio. The second was to decrease the size of the bars while maintaining the same number of bars. The first option was chosen for the flexural bars in the top of the cantilever. Seven No. 11 bars were used instead of eleven No. 11 bars. The second option was chosen for the shear reinforcement, skin reinforcement, and bottom flexural reinforcement. The spacing of this reinforcement, especially the shear reinforcement, could play a critical part in the response of the bent. To keep the spacing the same, the bar size was reduced from a No. 5 in the old bents to No. 4 in the new bents.

Tests were conducted to determine the yield strength of the reinforcement. The old reinforcement had a yield strength of approximately 43 ksi (296 MPa) while the new reinforcement had a yield strength of approximately 61.6 ksi (424 MPa).

The old bents were specified to have 3,000 psi (20,670 kPa) concrete. The new bents were also specified to have 3,000 psi (20,670 kPa) concrete. Four cylinders of concrete were cast when each bent was cast. The cylinders were left on site to cure by the side of the bents until the bents were tested. The cylinders were tested just after the bents were tested. The average compression strength of the cylinders was 4,305 psi (29,661 kPa). Because the compression strength of the new bents was more than that of the old bents, two cores were taken from Bent 12S. The tests of the cores resulted in an average compression strength of 5,600 psi (38,584 kPa), which was significantly higher than the specified concrete strength.

The influence of the yield strength of the reinforcement as compressive strength of the concrete will be discussed in Section 6.

The girder pedestals and shear keys shown schematically in Figure 3.4 were not cast on the new bents. Girder pedestals and shear keys provide no contribution to the structural performance of the bents therefore they were left off of the new bents.

The autopsy of the new bents showed that the concrete cover over the reinforcement was uneven on the sides of the bents. The bents, as shown in Figure 3.2, were cast on their sides; and as a result of neglect by the contractor, one inch (25.4 mm) spacers, rather than 2.5 inch (63.5 mm) spacers, were used on the bottom side of the form. Even though the old bents were not cast on their side, an identical situation was discovered on one of the old bents — one side had barely one inch (25.4 mm) cover while the other side had approximately four inches (101.6 mm). The authors of this report believe that the uneven side reinforcement cover, which was non code compliant, did not have any effect on the results of the research presented in this report because the mode of failure observed was flexure and the flexure reinforcement had code complaint cover. The small cover of the reinforcement along the side of the olds bents may be an explanation for the significant corrosion of the shear reinforcement along the sides of the bents.

# 4. Testing Methods

## 4.1 Test Frame

This section describes the model used to estimate forces necessary to test the bents, design of the testing frame, and concrete pad design.

A schematic drawing of the testing frame is shown in Fig. 4.1. In the diagram, the bent is laying on its side with a strong beam also lying on its side next to the bent. The frame clamps the portion of the bent opposite the cantilever against the strong beam. The testing apparatus allowed the cantilever portion of the bent to be loaded while using the strong beam to react the overall forces.

The frame was designed to load the bents resting on their side. Testing the bents on their side was necessary because of the position of the loading jacks and the members that would be in flexure due to the forces involved.

The loading capacity was also considered in the design of the frame. The actuators used in the testing were two PowerTeam 500-ton hydraulic jacks. Together the loading capacity of the jacks is 2,000 kips (8,900 kN). To be conservative, a load of this magnitude was used in designing the frame since the capacity of the old, new, and retrofitted bents was not exactly known.

### 4.1.1 Simple Model

A simple model of the system was developed using finite element (Visual Analysis, 1998) to determine forces on the testing frame. The simplified model of the system is shown in Figure 4.2. The bent was modeled as an infinitely stiff beam with a concentrated load of 2,000 kips (8,900 kN) on one end. The tension members were modeled as springs on the other end of the stiff beam, with a pinned connection at the center of rotation, 7.5 ft (2.3 m) from the point of application of the load. Several other models were developed to try to simulate what would happen during loading, none of which gave reasonable results.

The model shown in Figure 4.2 was analyzed to determine the forces and displacements of the members. Figure 4.3 shows the loads determined from the analysis. The most critical loads were 774 kips (3,444 kN) axial load in an exterior spring and 2,000 kips (8,900 kN) axial load as reaction.

### 4.1.2 Member Design

The maximum forces are transferred from the bent into several shear beams. These forces were transferred into tension members by steel beams. As a result of the short span, shear was the controlling factor in these beams. For the beams that supported the actuators, fabricated plate girders were designed with stiffeners at the locations of the point loads from the actuators and tension members. Wide flange beams were used to resist the clamping force on the end of the bent that was held fixed. Stiffeners were also placed in the wide flange beams at the locations of the tension members. Figure 4.4 shows the shear beam supporting the actuators.

The forces are transferred from the shear beams to the opposite set of shear beams by tension members, which were simply high strength steel bars. Dywidag bars were chosen for these tension members because they are round and threaded, making them easily attachable to the shear beams.

Two identical plate girders were borrowed from UDOT to act as the strong beam. The girders were welded together to provide the needed strength during testing.

### 4.1.3 Concrete Pad

A concrete pad was constructed to allow testing of the bents in the field. Figure 4.5 shows the pad constructed. The pad was designed to support the bent, shear beams, dywidags, and strong beam in place during testing.

The base of the pad was designed as a spread footing to support the weight of the bent, beams, and dywidags. The pad was made large enough to provide room for equipment and clearance around the bent. There are three steps on the top of the base pad. The bent was placed on the lowest step, in the foreground of Figure 4.5. The dywidags running through the step can also be seen in this figure. To align the strong beam with the bent, the step on the right in Figure 4.5 was made 6.5 in (165 mm) higher than the previous step. The highest step was designed to provide a tight fit between the bent and the shear beam.

Reinforcement for the pad was uniform throughout with No. 3 bars at 8 in (203 mm) on center. This provided the needed flexural strength for the pad, because it was designed as a footing. For simplicity, the reinforcing scheme was maintained through the whole pad.

Figure 4.6 shows the pad with strong beam, first bent, and shear beams in place.

### 4.2 Instrumentation

This section discusses the measurement of strain and displacement during testing. Steel and concrete strain gauges were used to measure strain. Linear Variable Differential Transformer Transducers (LVDT's) and string potentiometers (string pots) were used to measure displacement.

#### 4.2.1 Concrete Strain Gauges

The location and orientation of the concrete strain gauges are shown in Fig. 4.7. Strain gauges were placed on the two sides of the bent to measure the strain on the concrete. All four bents tested were instrumented with concrete strain gauges. Most of the gauges were oriented at 45º because this was thought to be the orientation of the maximum tensile strains (i.e., perpendicular to the cracks). The other gauges were oriented longitudinally on the beam.

The strain gauges had a gauge length of 90 mm and a gauge resistance of 120.3 (±0.5) ohms. A strain gauge is shown in Figure 4.8.

The strain gauges were mounted by first cleaning the concrete and, where needed, smoothing with a masonry grinder. Devcon 5-minute epoxy was applied, then sanded to create a smooth surface on which to attach the strain gauges. The strain gauges were then bonded onto the epoxy using the strain gauge adhesive, supplied by the manufacturer of the gauges. In using this method of mounting, the strain of the epoxy was assumed to be equal to the strain of the concrete. No tests were conducted to verify this assumption, however, this mounting method is the standard practice. Figure 4.9 shows a mounted strain gauge.

Several strain gauges were damaged prior to or during testing. Due to the fragile nature of the gauges occasionally gauges were torn off when the bents were set on the concrete pad by the crane, used to place the specimens in the testing frame. If possible, these gauges were replaced before testing, however, some gauges were inaccessible.

#### 4.2.2 Rebar Strain Gauges

The locations of the strain gauges on the reinforcement are shown in Figure 4.10. In the two new bents, the main reinforcement and shear reinforcement was instrumented with several strain gauges. Strain gauges were also placed on the skin

reinforcement and bottom reinforcement to provide a distribution of strain through selected cross sections. On the main flexural reinforcement, the gauges were placed at 1 ft (305 mm) on center beginning one foot (305 mm) from the end of the bar. On the shear reinforcement the gauges were placed at the quarter points along the height.

Two sizes of strain gauges were used: one for the No. 11 bars and one for the No. 4 bars. The larger strain gauges had a gauge length of 6 mm and a gauge resistance of 120 (±0.5) ohms. One of the larger strain gauges is shown in Figure 4.11. The smaller strain gauges had a gauge length of 3 mm and a gauge resistance of 120 (?0.5) ohms.

The rebar was prepared by grinding off the deformations in the area of the gauge and then sanding until a smooth surface was obtained. The strain gauges were attached with the adhesive provided by the manufacturer. As shown in Figure 4.12, waterproof strain gauges were used because the rebar would be exposed to water. The waterproof covering, however, had to be slightly trimmed for use on the small diameter bars as shown in Figure 4.13. Such trimming should not harm the waterproof qualities of the strain gauge.

Some of the strain gauges were damaged during construction of the bents despite the best efforts of the workers to not harm them. To provide access after casting, the lead wires of the strain gauges were pulled out through holes in the forms of the bent. As the forms were pulled off, several lead wires broke near the surface of the concrete. The wires were spliced with new wires after chipping away a small area of concrete around the wire, as shown in Figure 4.14.

### 4.2.3 LVDT's

Several Linear Variable Differential Transducer (LVDT's) and string potentiometers (string pots) were used to record displacements during testing. Figures 4.15 and 4.16 show the locations of the LVDT's on the cantilever arm and on the testing frame, respectively. Table 4.1 summarizes the range and locations of each LVDT or string pot.

To measure displacement on the underside of the cantilever, SP2-SP7 and LV1-LV6 were used. The instruments were mounted at the quarter points of the span and at the tip of the cantilever. Three measurements were taken through the cross-section at these points as well, as shown in Figure 4.15.

Instruments were also placed around the frame to monitor the movement of the frame and bent during testing. As shown in Figure 4.16, movement was measured at the opposite end of the bent (LV7), the shear beam with the actuators (LV9), the shear beam opposite the actuators (LV10), the base of the bent column (LV8), and the loading point of the strong beam (SP1).

### 4.2.4 Load Cells

The load cells are Sensotec brand and have an accuracy of ±300 lbs (1,335 kN). One load cell was used on the first two tests, and two load cells were used on the last two tests. The load cells were mounted between the actuator and the bent, as shown in Figure 4.4.

## 4.3 Data Acquisition

Data acquisition was accomplished by an independent computer and MEGADAC 5414AC system. The MEGADAC system has 128 dedicated strain gauge channels and 24 dedicated LVDT/string pot channels.

For the testing of the old bents, 32 strain gauge channels and 17 LVDT/string pot channels were used. The testing of the new bents required 119 strain gauge channels and 17 LVDT/string pot channels. For all of the tests, the system took one reading per second.

## 4.4 Loading Protocol

The bents were loaded in a cyclic manner. Figure 4.17 shows the loading protocol. For the bents tested to failure, 80 kip (356 kN) steps were taken to a load of 400 kips (1,780 kN). After 400 kips (1,780 kN), the test was displacement controlled. The yield displacement was estimated at 320 kips (1,424 kN) by assuming a yield capacity of 600 kips (2,670 kN). The simple relationship $\frac{320}{x_{320}} = \frac{600}{x_{yield}}$ was used to determine the yield displacement from the measured displacement corresponding to the load of 320 kips (1,424 kN). This relationship assumes a linear pre-yield slope, which was verified during testing. After 400 kips (1,780 kN) the bent was then pushed to the first displacement level, which corresponded to the estimated yield displacement. The

bent was then pushed to two times the estimated yield displacement, then three times the estimated yield displacement and continuing until failure. Three cycles were used for each load/displacement level.

For specimens tested to yield, 80 kip (356 kN) steps were used to load the bents up to 560 kips (2,492 kN). These bents were loaded to introduce sufficient cracking for investigation in the next phase of the project.

The loading rate was manually controlled. The hydraulic oil pump only had an on/off switch. Consequently, there was only one loading rate. The load was maintained for about 5 minutes on the peak of the third push of every cycle. This allowed time for examination of the specimen cracks, checking of instruments, reading of data manually as backup, and stabilization of the automatic instrument readings.

# 5. Test Results

Four bent specimens were cyclically tested. Table 5.1 shows the test matrix. These bents were designated 12N and 12S (N for north side of bent structure, S for South). The remaining two bents were new construction, being constructed during the summer of 2000. These bents were designated 1N and 2N (N for "New construction"). Bents 12S and 1N were tested to failure, failure being defined as a significant decrease in the peak load from one cycle to the next. Testing of Bents 12S and 1N revealed the yield point to be between 585 (2,603) and 625 kips (2,781 kN). Bents 12N and 2N were tested to a load of 560 kips (2,492 kN) to avoid significant damage since these bents will be retrofitted and retested again at a later date.

## 5.1 Monitoring of Test Frame

Overall, the testing frame performed well. A few minor problems appeared, caused by rigid body motion, but these were easily solved and accounted for during analysis of the data.

Wood shims were initially used between the bent and the frame, as shown in Figure 5.1. Due to the high loads during testing, the wood was crushed and the specimen experienced large rigid body movement. This was taken into account and corrected in the data by assuming a linear slope in the pre-yield portion of the load-deflection response. This assumption was validated by later tests showing the linear pre-yield portion of the load vs. deflection curve. On subsequent tests, steel shims were used. The steel shims significantly reduced the rigid body movement. An LVDT was also placed at the base of the column portion of the bent, as shown in Figure 4.16, to measure any movement taking place at the shim location during testing.

During the first test, only two sets of the five shear beam sets were actively engaged in clamping the bent. Figure 5.1 shows shear beam set numbers 1 and 2 as the active sets. Because of the wood shims crushing, the large rigid body motion made three of the five shear beam sets ineffective in restraining the bent. The steel shims helped to solve this problem on subsequent tests.

The sequence of prestressing the dywidags was also changed to help solve this problem. Initially, to create a more rigid test frame and to minimize settling of the frame during testing, the dywidag bars holding the opposite end of the bent were prestressed

before each test. This created a clamping force on the bent during testing. On the first test, the dywidags were prestressed from shear beam set No. 5 to No. 1. This sequence is from near the center of rotation to farther away from the center of rotation (assuming a center of rotation about the base of the column). Because the shear beam sits farther from the center of rotation have a greater moment arm, the bent moves in reducing the prestress in the shear beam sets closer to the center of rotation. The opposite sequence preserves the prestress in the dywidags prestressed first. Therefore, on all subsequent tests, the dywidags were prestressed from shear beam set No. 1 to No. 5.

Another problem encountered during the first test involved the shear beam holding the actuators. Figure 4.4 shows the setup of the actuator on the shear beam. Due to some eccentricity in the loading, the top end of the beam moved laterally when high loads were applied. Figure 5.2 is a picture of the beam supporting the actuators showing the lateral movement to the left of the top of the beam from the centerline of the system. An attempt was made to solve this problem by securing the shear beam within 4 angles, 2 on each side, as shown in Figure 5.3. The angles were welded to the support for the shear beam, which was bolted to the concrete pad. This minimized the lateral movement but did not eliminate it.

Figures 5.4, 5.5, and 5.6 show the graphs of LV7, LV8 and SP1, respectively. Figure 3.16 shows the locations of these instruments. These measurements were taken during the testing to failure of Bent 1N. Figure 5.4 shows the maximum displacement of LV7 during testing, which was less than 0.5 in (12.7 mm). During the tests taken to yield, the maximum movement was less than 0.3 in (7.6 mm). This is due to a lower peak load during the tests to yield. Figure 5.5 shows the movement at the base of the column. The maximum movement was 0.4 in (10.2 mm). Figure 5.6 shows that the strong beam deflected approximately 0.3 in (7.6 mm). Shifts of the strong beam are also evident in the graph during the loading due to rigid body motion.

### 5.2 Data Reduction

Each test lasted for several hours, creating large amounts of data. To reduce this data to a manageable amount, the average of every four values was taken. All graphs and tables have been produced from this data.

Three deflection measurements were taken through each cross section as seen in Figure 4.15. These values were averaged for presentation of results.

To correct the displacement due to rigid body motion, LV7 and LV8 were subtracted from the total deflection. The center of rotation for rigid body motion was assumed to be the bottom left corner of the bent column. LV7 was located the same distance from this point as the tip of the cantilever. The rigid body motion attributed to displacement at the tip was then equal to the rigid body motion at LV7. This assumption allowed LV7 to be directly subtracted. LV8 was the movement of the column toward or away from the strong beam. This enabled LV8 to also be directly subtracted. These corrections are reflected in the "corrected" version of each graph.

### 5.3 Bents Constructed in 1963

This section describes the test results and observations for the two old bents: Bent 12S, tested to failure, and Bent 12N, tested to yield.

#### 5.3.1 Bent 12S - Failure

The first bent tested was Bent 12S, which was severely deteriorated on the underside of the cantilever. As shown in Figure 5.7, several stirrups had corroded completely through and significant spalling of the concrete had occurred.

Table 5.2 shows the peak loads and deflections for each push of each cycle. The peak load of 709 kips (3,155 kN) occurred on the first push of cycle 13. The displacement at this load was 5.6 in (142 mm).

Figure 5.8 and 5.9 show the original and corrected load vs. displacement curves for Bent 12S, respectively. The curve was corrected by assuming a linear pre-yield stiffness and by subtracting LV7. The yield point of 625 kips (2,781 kN) is evident in these graphs. After yield, the permanent displacement is shown by the distance between the loading slope of one cycle and the unloading slope of the next cycle. The gap after cycle 10 is due to data that was deleted due to a short in the load cell.

The envelope curve of each push is shown in Figure 5.10. The stiffness of each push is very similar until the yield point. After the yield point, the second and third stiffnesses are similar, but less than the stiffness of the first push.

Cracking was first observed on the first push of cycle 4, at a load of 320 kips (1,424 kN). The first cracks to develop were in the reentrant corners of the girder pedestals, which are indicated in Figure 5.11. These cracks were hairline cracks due to the concentration of stress at the reentrant corner and did not extend into the cross

section. As loading progressed, the cracks in the reentrant corners began to lengthen into the cross section of the bent. On cycle 5, at a peak load of 400 kips (1,780 kN), another crack developed midway between the pedestals. These cracks are shown in Figure 5.12. The cracks extend several inches into the cross section.

On cycle 6, at a peak load of approximately 510 kips (2,270 kN), more cracks developed and two of them extended through more than half of the cross-section as shown in Figure 5.13. Figure 5.14 shows the direction of all cracks, which lengthened toward the reentrant corner of the column and cantilever. The bent apparently yielded on cycle 7, with a peak load during this cycle of 625 kips (2,781 kN) and a corresponding deflection of 0.81 in (21 mm). The cracks extending through most of the cross-section did not lengthen, as shown in Figure 5.15. Two other cracks extended to the length of the original longer cracks.

On cycle 8, with a peak load of approximately 640 kips (2,840 kN), no new cracks appeared. The existing cracks are shown in Figure 5.16. These cracks extended a few inches further toward the reentrant corner. On cycle 9, also with a peak load of 640 kips (2,840 kN), a new crack developed on the upper portion of the cantilever beam. The previous cracks extended to within a couple of inches of the bottom of the cantilever beam, as shown in Figure 5.17. After cycle 9, existing cracks became wider and did not lengthen with each successive loading. As shown in Figure 5.18, the main cracks eventually widened to between 0.25 (6.4) and 0.375 in (9.5 mm).

The bent reached a maximum load of 709 kips (3,155 kN) on the first push of cycle 13. After yielding, crushing of the concrete in the compression zone of the cross-section began and continued until failure. Figure 5.19 shows the crack pattern after failure and Figure 5.20 shows the compression zone after failure.

### 5.3.2 Bent 12N - Yield

Bent 12N was also severely deteriorated on the underside of the cantilever portion, although not as severely as Bent 12S. Figure 5.21 shows the cantilever beam and the deterioration on the underside of the beam. Severe spalling had occurred exposing some of the stirrups that were significantly corroded.

For the purposes of the overall project, Bent 12N was tested to just under the yield point. The yield point in the failure of Bent 12S was determined to be about 625 kips (2,781 kN). To approach the yield point, but not pass it, Bent 12N was taken to 560 kips (2,492 kN), in 80 kip (356 kN) increments, according to the loading protocol.

Table 5.3 shows the peak loads and displacements for every push of each cycle. The deflection at the peak load of approximately 560 kips (2,492 kN) was 0.8 in (20 mm).

Figures 5.22 and 5.23 show the original and corrected load vs. displacement curves for Bent 12N. The linear pre-yield slope of the curve is evident in these graphs.

Figure 5.24 shows the envelope curve of each push. The stiffnesses of each push are approximately equal.

There was one existing crack, shown in Figure 5.21, on the side of the bent before the test. The crack runs longitudinally down the main axis of the cantilever beam. A possible explanation for this crack is the expansion of the top rebar as it is corroded.

Bent 12N first showed signs of cracking in the reentrant corner of one of the pedestals beginning on cycle 4 at a peak load of 327 kips (1,455 kN). The crack was evident on the top of the bent but did not extend into the cross section. On cycle 5, with a peak load of 408 kips (1,816 kN), cracks on the top appeared at the other reentrant corners and at the third points between the two pedestals. These cracks are shown in Figure 5.25. These cracks also extended several inches into the cross section, with the exception of the crack aligned with the column face, which extended about halfway through the cross section meeting the preexisting crack.

On cycle 6, at a peak load of 480 kips (2,136 kN), two more cracks began to extend approximately halfway into the cross section, as shown in Figure 5.26. One of these cracks appeared from the column side of the cross section, angling toward the reentrant corner of the column and beam.

Cycle 7 was the last cycle of the test. The peak load on this cycle was 563 kips (2,505 kN). The three main cracks extended several inches toward the reentrant corner of the beam and column, as shown in Figure 5.27. A new crack extended from one of the reentrant corners through approximately ¾ of the cross section. All cracks completely closed upon unloading after each push.

### 5.4 Bents Constructed in 2000

This section describes the test results and observations for the new bents: Bent 1N, tested to failure, and Bent 2N, tested to yield.

### 5.4.1 Bent 1N - Failure

Table 5.4 shows the peak loads and displacements for every push of each cycle. The peak load occurred on cycle 9 with a load of 708 kips (3,151 kN) and at a displacement of approximately 3.3 in (84 mm).

The original and corrected load vs. displacement curves are shown in Figures 5.28 and 5.29, respectively. The bent apparently yielded at a load of 590 kips (2,626 kN) and a corresponding displacement of 0.9 in (23 mm).

The envelope curve of each push is shown in Figure 5.30. The stiffnesses of each push are approximately the same until the yield point. After the yield point, the stiffnesses of the second and third push are approximately equal, but the stiffness of the first push is higher.

The longitudinal strains taken from the first push of each cycle can be seen in Figure 5.31. The strain distribution is through the height of the cross section 2 ft (61 cm) from the column face. The neutral axis can be seen where the curve crosses the zero strain axis. The tension zone can be seen in the top of the bent and compression zone in the bottom of the bent.

Figure 5.32 shows the strain gauge data from one of the main flexural bars. The load at which the concrete cracks is approximately 200 kips (890 kN). At this point the stress previously in the concrete is now concentrated in the reinforcement. The yield of the reinforcement can also be seen at approximately 2,000 microstrain. The strain gauge malfunctions immediately after yielding of the reinforcement and causes the irregular lines seen in the graph.

Bent 1N began to crack on the first push of cycle 3, at a peak load of 247 kips (1,099 kN). Three small cracks extended several inches into the cross section. Another crack extended about halfway into the cross section, as shown in Figure 5.33. Cracks were spread evenly across the top of the bent. On cycle 4, at a load of 325 kips (1,447 kN), two new cracks developed farther away from column than the previous four. These cracks are shown in Figure 5.34.

At a load of 407 kips (1,811 kN), cycle 5, another new crack formed, this time on the fixed end of the bent. At this load level, cracks extended several more inches into the cross section with three of them extending approximately ¾ of the way through the cross section. Figure 5.35 shows the cracking present at this stage. After this cycle, the testing became displacement controlled.

The bent yielded during cycle 6 at a displacement of approximately 0.9 in (23 mm), which corresponded to a load of 590 kips (2,626 kN). The cycle had a peak load of 604 kips. No new cracks developed; however, existing cracks extended several more inches into the cross section, as shown in Figure 5.36. On cycle 7, at a displacement of 2.0 in (51 mm) and a peak load of 648 kips (2,884 kN), crushing of the concrete began to occur in the reentrant corner of the column and beam. Figure 5.37 shows the concrete spalling in this region. At this point in the testing, all existing cracks had extended at least halfway through the cross section, with the three main ones extending to within one foot of the reentrant corner. No new cracks developed at this displacement level. The cracks at this displacement level are shown in Figure 5.38.

No new cracks developed on cycle 8, which corresponded to a displacement level of 2.9 in (74 mm) and a peak load of 687 kips (3,057 kN). The crushing of the concrete on the underside of the cantilever beam continued with the cracks slightly progressing toward the reentrant corner. The cracks on this cycle are shown in Figure 5.39.

The bent reached the maximum load on cycle 9 during a displacement level of 3.7 in (94 mm). This corresponds to 3 times the yield displacement. The maximum load for this bent was 708 kips (3,151 kN). No new cracks developed. The existing cracks continued to widen and extend toward the reentrant corner of the column and beam.

On the first push of cycle 10, a distinct thud was heard along with significant widening of one of the cracks. At this point the test was stopped to prevent damage to the instruments. Figure 5.40 shows the crack pattern at this point. Also shown is the extensive damage to the underside of the cantilever where significant spalling of the concrete occurred. Figure 5.41 shows the permanent deflection (no load) of Bent 1N. A line is drawn on the figure to indicate the original position of the bent. The permanent deflection was approximately 3.5 in (89 mm).

### 5.4.2 Bent 2N - Yield

Bent 2N was taken to just under yield, similar to Bent 12N. Table 5.5 shows the peak loads and deflections for every push of each cycle. The peak load during testing was 567 kips (2,523 kN), corresponding to a displacement of 0.5 in. (13 mm).

Figures 5.42, 5.43, and 5.44 are the original and corrected Load vs. Deflection graphs for Bent 2N. Similar to Bent 12N, the slope is linear through the duration of the test.

Figure 5.45 shows the envelope curve of each push. The stiffnesses of each push are approximately equal, showing no significant difference.

Figure 5.46 shows the strain distribution through the height of the cross section 2 ft (61 cm) from the column face. The strains were taken from the first push of each cycle. The neutral axis can be seen where the curve crosses the zero strain axis. The tension zone can be seen in the top of the bent and compression zone in the bottom of the bent.

On cycle 3, with a maximum load of 245 kips (1,090 kN), three cracks started to develop, as shown in Figure 5.47. One crack was in line with the edge of the column face and extended more than halfway through the cross section. The other two cracks were on either side of the longer crack and extended a few inches into the cross section.

Three new cracks developed on cycle 4, at a peak load of 325 kips (1,446 kN), as shown in Figure 5.48. One of these extended more than halfway through the cross section. The main crack, in line with the column face, extended another several inches.

On cycle 5, with a peak load of 402 kips (1,789 kN), two new cracks developed. Figure 5.49 shows the cracks on this cycle. Two of the cracks now were extended through approximately ¾ of the cross section. Most of the other cracks extended about halfway through the cross section.

On cycle 6, with a peak load of 485 kips (2,158 kN), no new cracks developed. The existing cracks, however, extended several inches through the cross section, as shown in Figure 5.50. The two longest cracks were within several millimeters of the bottom of the cantilever beam.

The last cycle had a peak load of 567 kips (2,523 kN). Two new cracks developed, as shown in Figure 5.51. The new cracks extended about 2 feet (51 cm) into the cross section. The two cracks closest to the reentrant corner did not extend any further during this cycle. The other major cracks, however, continued to propagate several more inches toward the corner.

# 6. Interpretation of Results

## 6. 1 Yield Load

Bent 12S and Bent 1N, the two bents tested to failure, yielded at different loads. The difference is most likely due to the change in reinforcement discussed in Section 3. The old bents had an area of main flexural reinforcement ($A_s$) of 17.16 $in^2$ (111 $cm^2$). Due to the difference in grade, the new bent area of main flexural reinforcement was equal to 2/3 of 17.16 (111) or 11.44 $in^2$ (74 $cm^2$). Seven No. 11 bars were used, providing an $A_s$ of 10.92 $in^2$ (71 $cm^2$). The ratio of reinforcement between the new and old bents is 0.91. If the measured yield load of the old bent is multiplied by this ratio, it is reduced so that the final yield load is approximately the measured yield load for the new bent. This adjusted yield load is shown in Table 6.1.

Figure 6.1 shows the longitudinal strain of a main flexural bar, measured 2 ft. (61 cm) from column face, for Bent 1N. The graph shows the reinforcement begin to yield. The yield load according to the load vs. displacement curve for that bent, shown in Figure 5.29, is approximately 590 kips (2,626 kN). According to the measured strains, shown in Figure 6.1, yielding of the main flexural reinforcement occurred approximately at the same 590 kip load (2,626 kN).

Figure 6.2 shows the strain along the length of the main flexural bars. The strain predicted by Bernoulli beam theory is plotted on the same graph. The strains have a similar slope but the measured strains are consistently higher along the length.

## 6.2 Moment Curvature

Using strain gauge data from the reinforcement in Bent 1N, the actual moment curvature was calculated. A linear strain profile was assumed between two strain gauge readings. The depth of the neutral axis could then be calculated. The curvature was then found by dividing the strain by the distance from the neutral axis.

Figure 6.3 shows the curvature on the first push of each cycle, along with the theoretical moment curvature discussed in Section 2. The pre-cracking stiffness, the cracking moment, and curvature at cracking agree well with each of the theoretical methods. The pre-yield stiffness and yield point shown by the hand calculations match well with those of the cross section. The respective stiffness and yield point of BIAX and Response vary slightly from the actual stiffness and yield point.

### 6.3 Yield Displacement

The calculated and measured yield displacements are shown in Table 6.2. Actual material properties were used during calculations of yield displacements. The calculated displacements compare well, but are slightly less than the measured displacements. This may be due to the neglect of a cracked cross section in calculating the shear deformation.

The difference between the yield displacements of the bents is due to the transition from grade 40 to grade 60 steel. Grade 40 reinforcement has less strain at yield than grade 60. This is evident because strain is equal to stress divided by the modulus of elasticity. The yield stress decreases and as a result, the yield strain decreases. A lower strain in the main flexural reinforcement will therefore cause the beam to deflect less.

### 6.4 Cracking

The new and old bents cracked on different cycles. The new bents cracked on the first push to approximately 240 kips (1,068 kN). The old bents each cracked on the first push to 400 kips (1,779 kN). The old bents also initially cracked in the reentrant corner of the girder pedestals. The new bents did not have girder pedestals and as a result cracking was spread somewhat evenly across the top of the bent, where the pedestals would normally be located.

The cracking pattern observed in the bents tested is very similar to that reported by Tan et al. (1997). Figure 6.4a shows the crack pattern for the deep beams tested by Tan and the bents tested by the author. The deep beam shown has a shear span to depth ration (a/d) of 1.5 while the cantilever portion of the bent has a ratio of 1.6. The major difference between the deep beams and the cantilever bent is the loading. The deep beams were loaded at the third points while the cantilever bent was loaded with a concentrated point load at the tip of the cantilever. By turning the bent upside down, as shown in Figure 6.4b, the cracking pattern of the shear span of both, the deep beam and the bent, are very similar.

The failure mode observed by Tan et al. (1997), is also similar to that observed during testing of the bents. For beams with a/d between 1.0 and 2.5, diagonal tension failure was the controlling failure. Diagonal tension failure is characterized by a large crack from the load point to the support. In figure 6.4a, the main crack is shown for one

of the deep beams. Both Bents 12S and 1N developed a large crack at failure (See Fig. 5.40) similar to those reported by Tan et al. (1997).

### 6.5 Longitudinal Strain Distribution

The strain distribution through the height of the cross section of Bents 1N and 2N are shown in Figures 5.31 and 5.46, respectively. As expected, the strain increases with increasing load. As shown in Figure 5.31, Strain Gauge No. 1006 did not work properly after yield; consequently, the post yield strain values were not recorded. Strain Gauge 1105 also seems to have inaccurate strain values through the complete test. If Strain Gauge No. 1105 is not included, interpolation between the other strain gauges indicates a somewhat linear strain distribution, similar to Strain Gauge No. 2220 in Figure 5.46. The strain distribution is not perfectly linear, however, as assumed in Bernoulli beam theory. This not quite linear strain distribution and the slightly underestimation of the yield load predicted by Bernoulli beam theory indicate that other factors may affect the behavior of the bents.

# 7. Conclusion

## 7.1 Conclusions

From this study, the following conclusions are made:

- Bernoulli beam theory gives a good approximation of the capacity of the reinforced concrete bents tested in this study. The strain distribution through the depth of the cross section can be approximated by a linear function, indicating that the response of the beam is controlled by Bernoulli beam theory. The reasonable idealization is also shown by the theoretical moment-curvature response, which agrees well with the actual moment-curvature response.
- Behavior of the bents is governed by flexure. According to the AASHTO provisions (1996), design is controlled by shear rather than by flexure. The tests conducted show; however, that flexure is the main mode of failure. Analysis methods for slender flexural beams will therefore better predict the capacity of bents than analysis methods for deep flexural beams.
- There are no D-Regions on the bents, which is evidenced by the linear strain distribution through the depth of the cross section of the bents. Because the shear reinforcement did not yield, the non linear stress-strain concrete relationship was not engaged to the point to govern the response of the bents. Thus, strut and tie models, which have been shown to estimate accurately the load capacity for regions of non linear strains distributions, did not accurately estimate the load capacity of the bents. Strut and tie models assume shear reinforcement yielding; as the shear reinforcement yields, the flexural capacity of the model is reached; as the flexural capacity is developed, the concrete becomes the controlling factor. For the bents tested, the compressive strength of the concrete was irrelevant because the concrete was not fully engaged. On the other hand, the flexural reinforcement was fully engaged eventually controlling the behavior of the bents. Since the actual values of the reinforcement yield strengths were very close to the values assumed during preliminary calculations, the predictions were very reasonable.
- Deterioration of the bents did not affect the capacity. This is because the main flexural reinforcement had not shown serious corrosion effects.
- Because the bents failed in flexure, a flexural strengthening may be warranted if capacity needs to be increased. A shear strengthening, on the other hand, is only

warranted if the flexural strengthening increases significantly the capacity of the bent such that shear capacity becomes extremely low and controls the design.

### 7.2 Recommendations

Based on the results of the tests conducted, the following recommendations are made to UDOT:

- Engineers may use the pictures contained in this report to visually determine the degree of deterioration of reinforced concrete cantilevered bent caps. If main flexural reinforcement is not significantly corroded the concrete deterioration and shear reinforcement corrosion will not affect the capacity of the bents. If main flexural reinforcement is significantly corroded, UDOT must conduct further research to determine the effects of corrosion on the response of the bents. As the main flexural reinforcement becomes significantly corroded, the response of the bents may no longer be governed by flexure.
- Engineers shall use the traditional beam analysis method to determine the capacity of reinforced concrete cantilevered bent caps if the main flexural reinforcement is not significantly corroded. The method is based on Bernoulli beam theory, is the method of design codes and is summarized in any reinforced concrete design book.
- Engineers wanting to increase the capacity of the bents may do so through a flexural strengthening scheme. A shear strengthening, on the other hand, is not warranted unless the flexural strengthening increases significantly the capacity of the bent such that shear capacity becomes extremely low and controls the design. UDOT must conduct further research to determine appropriate flexural and shear strengthening procedures.

### 7.3 Benefits

UDOT engineers can use the results of this research when determining whether or not deteriorated reinforced concrete cantilevered bent caps actually need to be repaired. As determined by the results of this research, capacity is not compromised if the main flexural reinforcement is not significantly corroded. If capacity is not compromised, a cosmetic retrofitting is all that is needed. Recommendations if capacity is compromised by main flexural reinforcement corrosion are beyond the scope of this report.

## 8. References


ACI-ASCE Committee 426, “The Shear Strength of Reinforced Concrete Members,” Chapter 1 to 4, Proceedings, ASCE, V.99, No. ST6, June 1973, pp.1148-1157

BIAX; Wallace, John W.; Moehle, Jack P., Department of Civil Engineering, University of California at Berkeley, California; July 1989

“Building Code Requirements for Structural Concrete and Commentary,” American Concrete Institute, 1999

Chow, Li; Conway, Harry; and Winter, George, “Stresses in deep Beams,” Transactions, ASCE, V.118, 1953, pp. 686-708.

Collins, Micheal P.; Mitchell, Denis; “Prestressed Concrete Structures,” Prentice Hall, 1990

Crist, R.A., “Shear Behavior of Deep Reinforced Concrete Beams,” Proceedings, Symposium on the Effects of Repeated Loading of Materials and Structural Elements (Mexico City, 1966), V.4, RILEM, Paris, 31 pp. (Published by Instisto Mexicano del Cemento y del Concrete, Mexico D.F., Mexico)

De Paiva, H.A.R.; Seiss, C.P., “Strength and Behavior of dep Beams in Shear,” Proceedings, ASCE, V.91, ST5, Part 1, Oct. 1965, pp.19-41

Ferguson, Phil M., “Reinforced Concrete Fundamentals,” John Wiley and Sons, New York, 1965

Kesner, Keith E.; Poston, Randall W.; “Truss Models in Detailing,” *Concrete International*, Nov. 2000, pp. 48-54

MacGregor, James M., “Reinforced Concrete Mechanics and Design,” Prentice Hall, New Jersey, 1997

Marti, Peter, “Truss Models in Detailing,” *Concrete International*, Dec. 1985, pp. 66-73

Park, R.; Paulay, T., “Reinforced Concrete Structures,” Wiley-Inter-Science, New York, 1975, 769 pp.

Portalnd Cement Association, “Design of Deep Beams,” ISO79D, 1946, 10pp.

Rogowsky, David M.; MacGregor, James G.; Ong, SeeY., “Test of Reinforced Concrete Deep Beams,” *ACI Journal*, Vol. 83, No. 4, July-August 1986a, pp. 614-623

Rogowsky, David M.; MacGregor, James G., “Design of Reinforced Concrete Deep Beams,” *Concrete International*, Vol. 8, No. 8, Aug. 1986b, pp. 49-58

“Standard Specifications for Highway Bridges,” American Association of State Highway and Transportation Officials, 1996

"Standard Specifications for Highway Bridges," American Association of State Highway Officials, 1961

Tan, Kang-Hai; Tang, Susanto; Kong, Fung-Kew; Lu, Hai-Yun, "Main Tension Steel in High Strength Concrete Deep and Short Beams," *ACI Structural Journal*, Vol. 94, No. 6, November-December 1997, pp. 752-768

Visual Analysis, Integrated Engineering Software, Inc., 1998

## Tables

Table 2.1 – USD, WSD, and moment curvature capacities

| | | Shear (kips) | | Corresponding to a load of: | | Flexure (kip-ft) | | Corresponding to a load of: | |
|---|---|---|---|---|---|---|---|---|---|
| | | Kips | kN | Kips | kN | Kip-ft | kN-m | Kips | kN |
| WSD | | 226 | 1006 | 226 | 1006 | 1426 | 1933 | 228 | 1015 |
| USD | | 476 | 2118 | 476 | 2118 | 3028 | 4105 | 484 | 2154 |
| Moment Curvature | Response | --- | --- | --- | --- | 3144 | 4263 | 740 | 3292 |
| | BIAX | --- | --- | --- | --- | 2757 | 3738 | 649 | 2887 |
| | Hand Calcs. | --- | --- | --- | --- | 2514 | 3409 | 592 | 2632 |

Table 2.2 – Calculated Yield Displacements

| | Bernoulli beam theory | | Timoshenko beam theory | |
|---|---|---|---|---|
| | in | mm | in | mm |
| **Existing Bents** | 0.59 | 14.99 | 0.63 | 16.00 |
| **New Bents** | 0.81 | 20.57 | 0.85 | 21.59 |

Table 2.3 – Strut and tie model matrix

| Model | # of Active Stirrups | Main Steel at Yield? |
|---|---|---|
| **1** | 0 | Yes |
| **2** | 2 | Yes |
| **3** | 3 | Yes |
| **4** | 4 | Yes |
| **5** | 5 | Yes |
| **6** | 7 | No |

Table 2.4 – Results of strut and tie models

| Model | Point Load at Yield | | Load on Main Compression Strut | |
|---|---|---|---|---|
| | Kips | kN | Kips | kN |
| **1** | 425 | 1891 | 781 | 3475.45 |
| **2** | 441 | 1962 | 568 | 2527.6 |
| **3** | 432 | 1922 | 446 | 1984.7 |
| **4** | 431 | 1918 | 316 | 1406.2 |
| **5** | 429 | 1909 | 203 | 903.35 |
| **6** | 440 | 1958 | --- | --- |

Table 4.1 – Displacement LVDT's and String pots

| Name | Range | | Measuring displacement of: |
|---|---|---|---|
| **LV1** | ±6 in. | ±153 mm | cantilever arm |
| **LV2** | ±6 in. | ±153 mm | cantilever arm |
| **LV3** | ±6 in. | ±153 mm | cantilever arm |
| **LV4** | ±6 in. | ±153 mm | cantilever arm |
| **LV5** | ±6 in. | ±153 mm | cantilever arm |
| **LV6** | ±6 in. | ±153 mm | cantilever arm |
| **LV7** | ±6 in. | ±153 mm | clamped end of bent |
| **LV8** | ±2 in. | ±51mm | column of bent |
| **LV9** | ±6 in. | ±153 mm | shear beam with actuators |
| **LV10** | ±2 in. | ±51 mm | shear beam with strong beam |
| **SP1** | ±10 in. | ±254 mm | strong beam |
| **SP2** | ±10 in. | ±254 mm | cantilever arm |
| **SP3** | ±10 in. | ±254 mm | cantilever arm |
| **SP4** | ±10 in. | ±254 mm | cantilever arm |
| **SP5** | ±10 in. | ±254 mm | cantilever arm |
| **SP6** | ±10 in. | ±254 mm | cantilever arm |
| **SP7** | ±10 in. | ±254 mm | cantilever arm |

Table 5.1 – Test Matrix

| Bent Designation | Construction | Fail or Yield? |
|---|---|---|
| Bent 12S | 1963 | Fail |
| Bent 12N | 1963 | Yield |
| Bent 1N | 2000 | Fail |
| Bent 2N | 2000 | Yield |

Table 5.2 – Peak Loads and Displacements for Bent 12S

| Bent 12S | First Push | | | | Second Push | | | | Third Push | | | |
|---|---|---|---|---|---|---|---|---|---|---|---|---|
| | Load | | Disp. | | Load | | Disp. | | Load | | Disp. | |
| | Kips | kN | In | mm | Kips | kN | In | mm | Kips | kN | In | mm |
| **Cycle 1** | 81 | 359 | 0.13 | 3.38 | 81 | 362 | 0.14 | 3.58 | 84 | 373 | 0.15 | 3.86 |
| **Cycle 2** | 162 | 719 | 0.13 | 3.38 | 160 | 713 | 0.19 | 4.71 | 166 | 737 | 0.21 | 5.31 |
| **Cycle 3** | 240 | 1068 | 0.22 | 5.60 | 246 | 1093 | 0.29 | 7.44 | 248 | 1105 | 0.32 | 8.09 |
| **Cycle 4** | 321 | 1428 | 0.23 | 5.74 | 322 | 1434 | 0.28 | 7.00 | 323 | 1439 | 0.30 | 7.61 |
| **Cycle 5** | 399 | 1774 | 0.30 | 7.72 | 401 | 1783 | 0.37 | 9.42 | 401 | 1786 | 0.40 | 10.27 |
| **Cycle 6** | 511 | 2274 | 0.44 | 11.13 | 487 | 2166 | 0.48 | 12.09 | 488 | 2171 | 0.49 | 12.35 |
| **Cycle 7** | 625 | 2783 | 0.81 | 20.50 | 604 | 2686 | 0.98 | 24.94 | 598 | 2662 | 0.99 | 25.06 |
| **Cycle 8** | 641 | 2852 | 1.47 | 37.31 | 603 | 2682 | 1.49 | 37.87 | 596 | 2651 | 1.49 | 37.95 |
| **Cycle 9** | 641 | 2854 | 2.00 | 50.81 | 606 | 2698 | 2.04 | 51.91 | 603 | 2685 | 2.04 | 51.92 |
| **Cycle 10** | 665 | 2959 | 2.96 | 75.20 | 626 | 2786 | 2.97 | 75.35 | 623 | 2772 | 2.97 | 75.47 |
| **Cycle 11** | 695 | 3094 | 3.93 | 99.76 | 653 | 2904 | 3.97 | 100.79 | 639 | 2844 | 3.96 | 100.69 |
| **Cycle 12** | 703 | 3126 | 4.96 | 126.03 | 664 | 2955 | 4.96 | 126.11 | 650 | 2893 | 4.95 | 125.65 |
| **Cycle 13** | 709 | 3156 | 5.64 | 143.36 | 652 | 2900 | 5.96 | 151.39 | 636 | 2830 | 5.96 | 151.41 |
| **Cycle 14** | 696 | 3096 | 6.31 | 160.22 | 597 | 2655 | 6.95 | 176.49 | 562 | 2500 | 6.97 | 176.97 |

Table 5.3 – Peak Loads and Displacements for Bent 12N

| Bent 12N | First Push | | | | Second Push | | | | Third Push | | | |
|---|---|---|---|---|---|---|---|---|---|---|---|---|
| | Load | | Disp. | | Load | | Disp. | | Load | | Disp. | |
| | Kips | kN | in | mm | Kips | kN | in | mm | Kips | kN | in | mm |
| **Cycle 1** | 89 | 396 | 0.02 | 0.63 | 91 | 406 | 0.05 | 1.37 | 91 | 403 | 0.06 | 1.61 |
| **Cycle 2** | 165 | 165 | 0.13 | 0.13 | 165 | 734 | 0.15 | 3.90 | 164 | 729 | 0.16 | 4.15 |
| **Cycle 3** | 240 | 243 | 0.22 | 0.22 | 243 | 1081 | 0.24 | 6.08 | 248 | 1103 | 0.26 | 6.53 |
| **Cycle 4** | 322 | 327 | 0.35 | 0.35 | 327 | 1454 | 0.34 | 8.61 | 324 | 1440 | 0.34 | 8.64 |
| **Cycle 5** | 400 | 402 | 0.42 | 0.42 | 402 | 1789 | 0.43 | 11.00 | 408 | 1815 | 0.44 | 11.11 |
| **Cycle 6** | 478 | 478 | 0.57 | 0.57 | 478 | 2129 | 0.61 | 15.39 | 480 | 2135 | 0.62 | 15.87 |
| **Cycle 7** | 559 | 562 | 0.74 | 0.74 | 562 | 2502 | 0.76 | 19.36 | 563 | 2505 | 0.79 | 20.08 |

Table 5.4 – Peak Loads and Displacements for Bent 1N

| Bent 1N | First Push | | | | Second Push | | | | Third Push | | | |
|---|---|---|---|---|---|---|---|---|---|---|---|---|
| | Load | | Disp. | | Load | | Disp. | | Load | | Disp. | |
| | Kips | kN | in | mm | Kips | kN | in | mm | Kips | kN | in | mm |
| **Cycle 1** | 82 | 364 | 0.12 | 3.16 | 94 | 417 | 0.15 | 3.74 | 89 | 397 | 0.15 | 3.81 |
| **Cycle 2** | 157 | 701 | 0.21 | 5.30 | 164 | 728 | 0.22 | 5.61 | 162 | 722 | 0.18 | 4.63 |
| **Cycle 3** | 247 | 1099 | 0.22 | 5.57 | 248 | 1104 | 0.29 | 7.42 | 247 | 1098 | 0.36 | 9.09 |
| **Cycle 4** | 325 | 1444 | 0.40 | 10.14 | 326 | 1453 | 0.43 | 10.87 | 319 | 1421 | 0.40 | 10.20 |
| **Cycle 5** | 406 | 1807 | 0.59 | 15.06 | 407 | 1810 | 0.62 | 15.85 | 404 | 1799 | 0.63 | 16.03 |
| **Cycle 6** | 604 | 2686 | 1.13 | 28.77 | 561 | 2497 | 1.15 | 29.14 | 547 | 2432 | 1.15 | 29.20 |
| **Cycle 7** | 648 | 2885 | 1.97 | 49.91 | 602 | 2681 | 2.02 | 51.32 | 594 | 2645 | 2.03 | 51.44 |
| **Cycle 8** | 687 | 3057 | 2.84 | 72.10 | 646 | 2876 | 2.89 | 73.30 | 631 | 2809 | 2.88 | 73.18 |
| **Cycle 9** | 708 | 3152 | 3.25 | 82.67 | 609 | 2711 | 3.71 | 94.14 | 588 | 2618 | 3.72 | 94.57 |
| **Cycle 10** | 617 | 2744 | 3.94 | 100.14 | | | | | | | | |

Table 5.5 – Peak Loads and Displacements for Bent 2N

| Bent 2N | First Push | | | | Second Push | | | | Third Push | | | |
|---|---|---|---|---|---|---|---|---|---|---|---|---|
| | Load (kips) | | Disp. | | Load (kips) | | Disp. | | Load (kips) | | Disp. | |
| | Kips | kN | in | mm | Kips | kN | in | mm | Kips | kN | in | mm |
| **Cycle 1** | 79 | 351 | 0.00 | 0.00 | 89 | 396 | 0.01 | 0.26 | 87 | 385 | 0.01 | 0.26 |
| **Cycle 2** | 162 | 723 | 0.01 | 0.18 | 165 | 736 | 0.00 | 0.08 | 163 | 726 | 0.01 | 0.16 |
| **Cycle 3** | 244 | 1087 | 0.06 | 1.60 | 243 | 1081 | 0.07 | 1.81 | 245 | 1091 | 0.08 | 2.14 |
| **Cycle 4** | 321 | 1430 | 0.20 | 5.02 | 325 | 1445 | 0.19 | 4.85 | 323 | 1437 | 0.20 | 5.09 |
| **Cycle 5** | 402 | 1791 | 0.27 | 6.84 | 401 | 1784 | 0.27 | 6.75 | 401 | 1783 | 0.27 | 6.84 |
| **Cycle 6** | 482 | 2144 | 0.36 | 9.24 | 485 | 2158 | 0.36 | 9.05 | 483 | 2149 | 0.37 | 9.33 |
| **Cycle 7** | 565 | 2514 | 0.48 | 12.19 | 567 | 2523 | 0.46 | 11.80 | 567 | 2521 | 0.48 | 12.07 |

Table 6.1 – Bent 12S and 1N, predicted and adjusted yield loads

| | Predicted by USD | | Measured | | Adjusted Measured | | Failure | |
|---|---|---|---|---|---|---|---|---|
| | Kips | kN | Kips | kN | Kips | kN | Kips | kN |
| **Bent 12S** | 484 | 2154 | 625 | 2781 | 625 | 2781 | 709 | 3155 |
| **Bent 1N** | 464 | 2065 | 588 | 2617 | 646 | 2875 | 708 | 3151 |

Table 6.2 - Bent 12S and 1N, predicted and measured yield displacements

| | Bernoulli beam theory | | Timoshenko beam theory | | Measured Displacement (in) | |
|---|---|---|---|---|---|---|
| | in | mm | in | mm | in | mm |
| **Bent 12S** | 0.59 | 14.99 | 0.63 | 16.00 | 0.78 | 19.81 |
| **Bent 1N** | 0.81 | 20.57 | 0.85 | 21.59 | 0.90 | 22.86 |

**Figures**

Figure 1.1 – Bent Caps 12, 13, and 14.

Figure 1.2 – Cantilever Portion of Bent 12.

Figure 1.3 – Bent 12S, deterioration on underside of cantilever

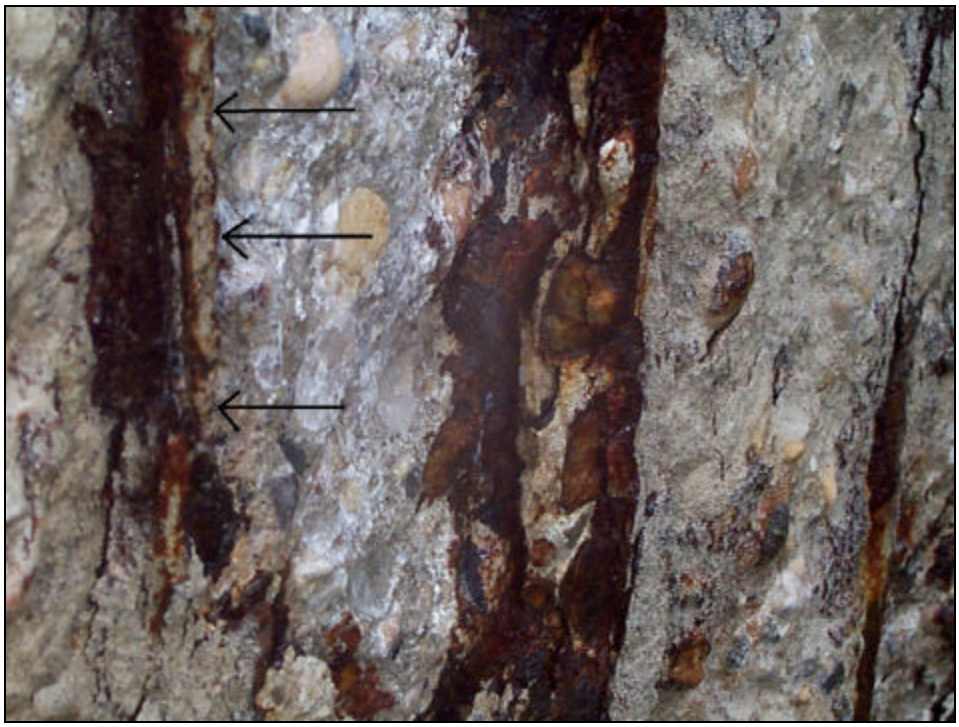

Figure 1.4 – Bent 12S, completely corroded stirrup

Figure 1.5 – Bent 12S, deterioration at tip of cantilever

Figure 1.6 – Bent 12N, close up of deterioration on underside of cantilever

Figure 1.7 – Bent 12N, deterioration on underside of cantilever

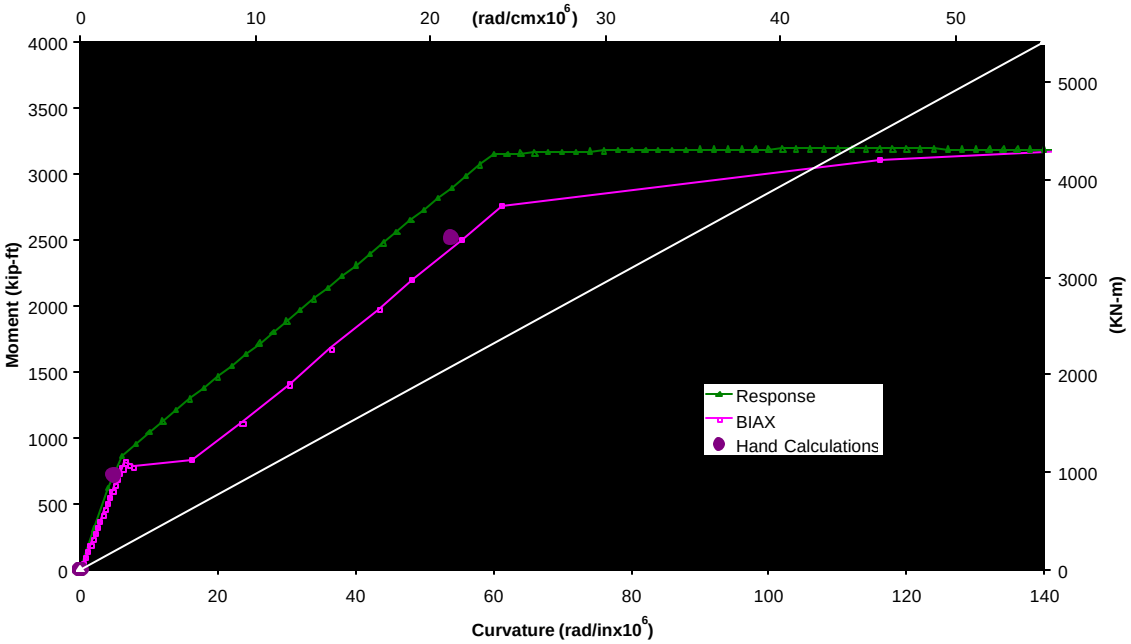


Figure 2.1 – Theoretical moment curvatures

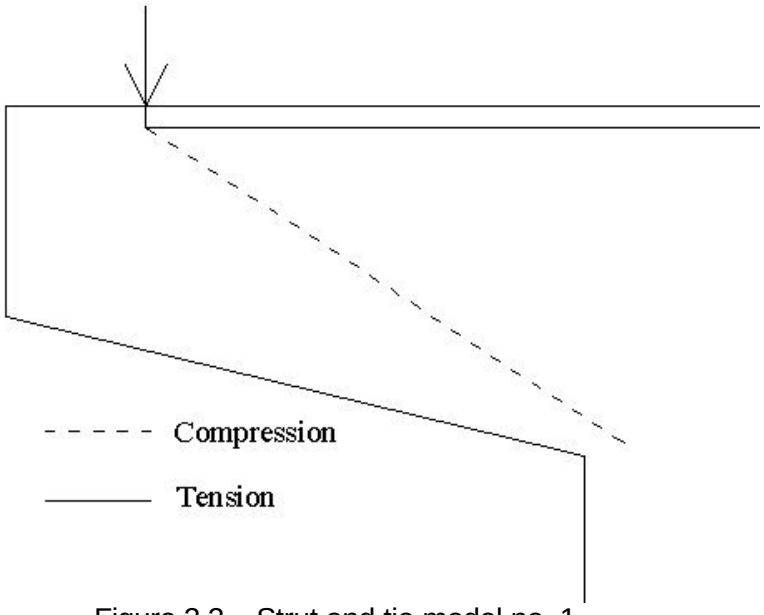


Figure 2.2 – Strut and tie model no. 1

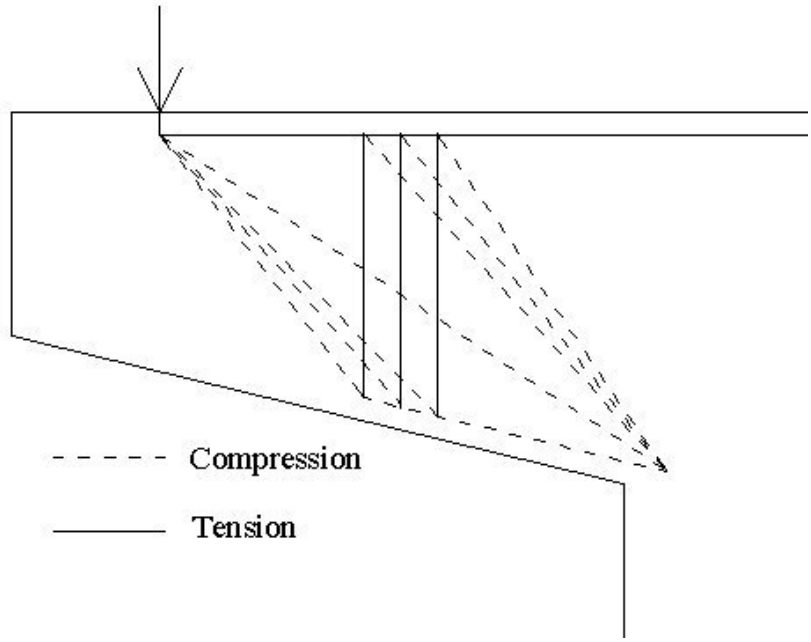


Figure 2.3 – Strut and tie model no. 3

Figure 3.1 – Reinforcement cage for new bent.

Figure 3.2 – Forms for new bent being cast on its side.

Figure 3.3 – New bent after removal of the forms.

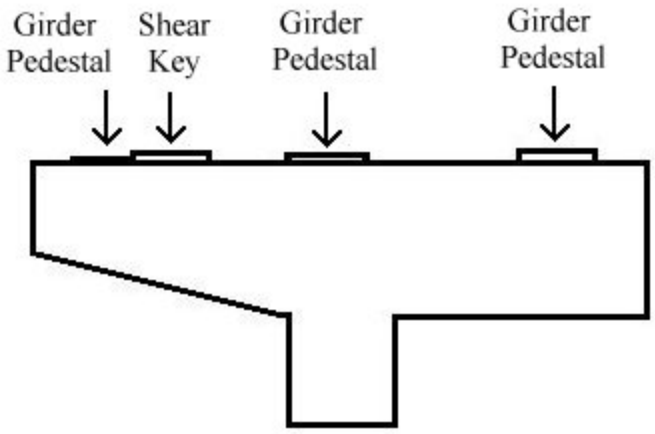


Figure 3.4 – Girder pedestals and shear key.

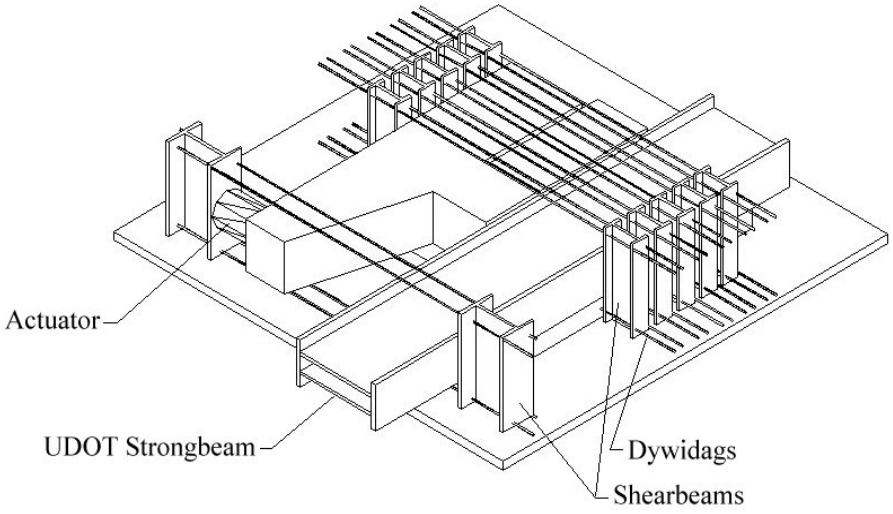


Figure 4.1 – Concept for Test Frame

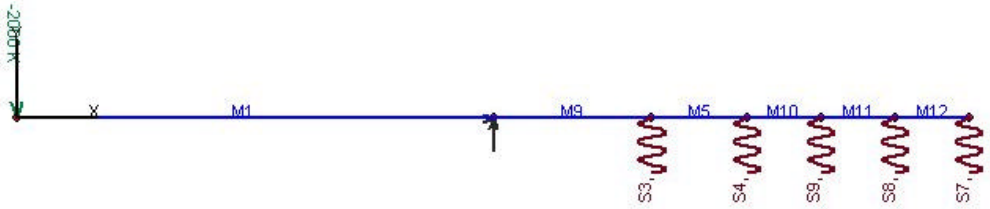


Figure 4.2 – Frame model created in visual analysis

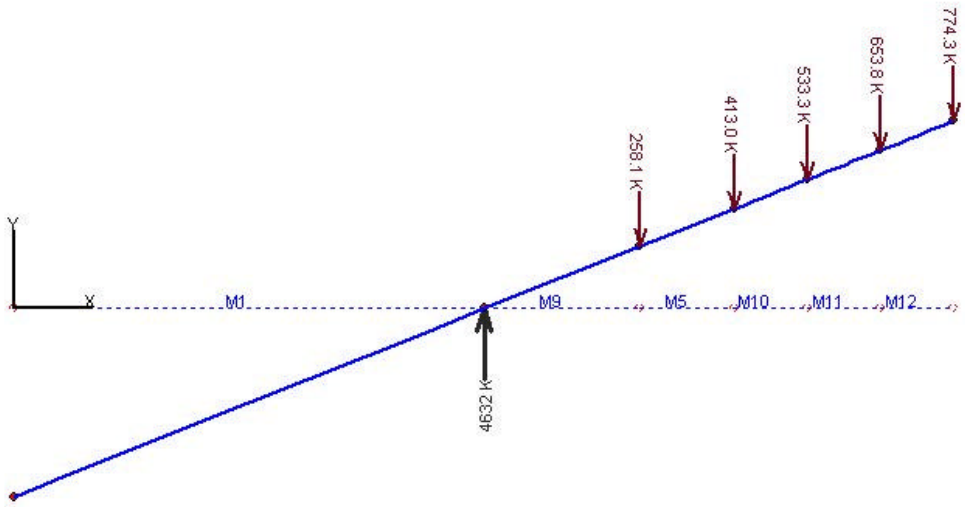


Figure 4.3 – Results of visual analysis model

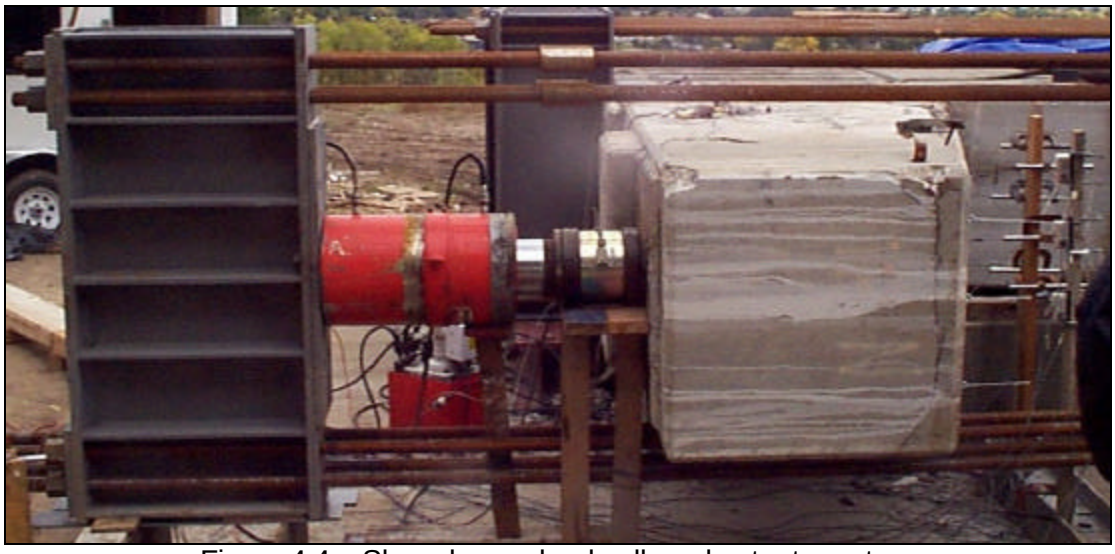

Figure 4.4 – Shear beam, load cell, and actuator setup.

Figure 4.5 – Constructed test pad

Figure 4.6 – Test frame without dywidags and first bent in place for testing.

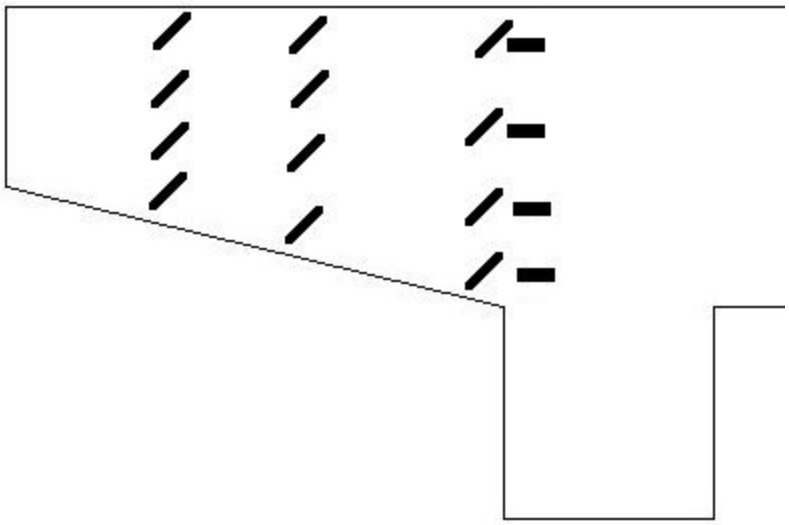

Figure 4.7 – Location of concrete strain gauges.

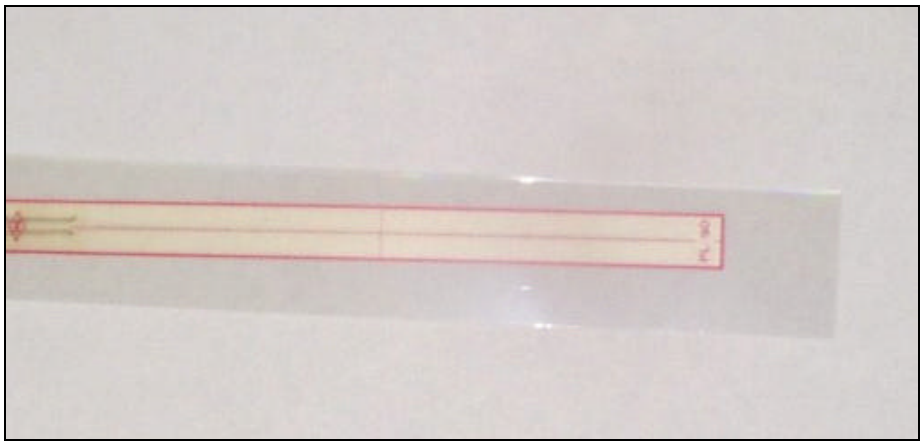

Figure 4.8 – Concrete strain gauge

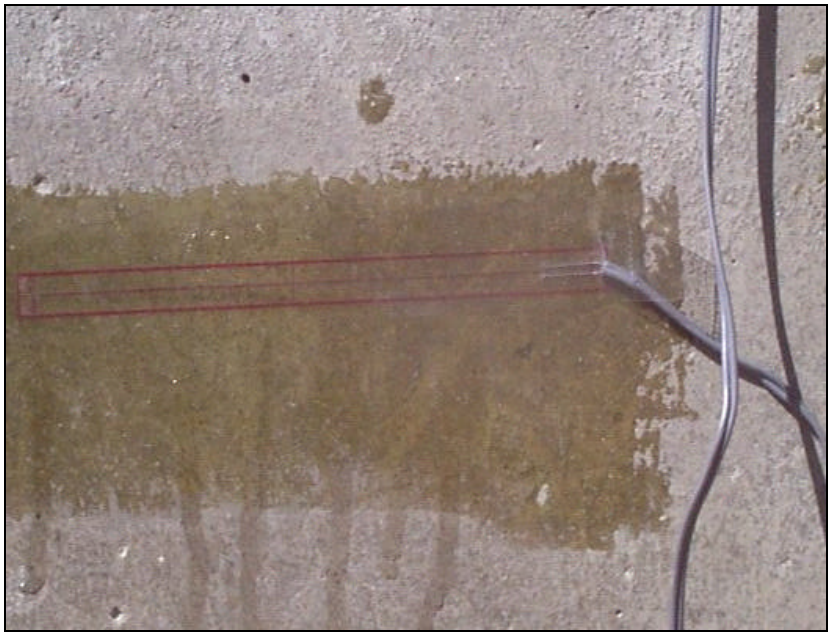

Figure 4.9 – Mounted concrete strain gauge

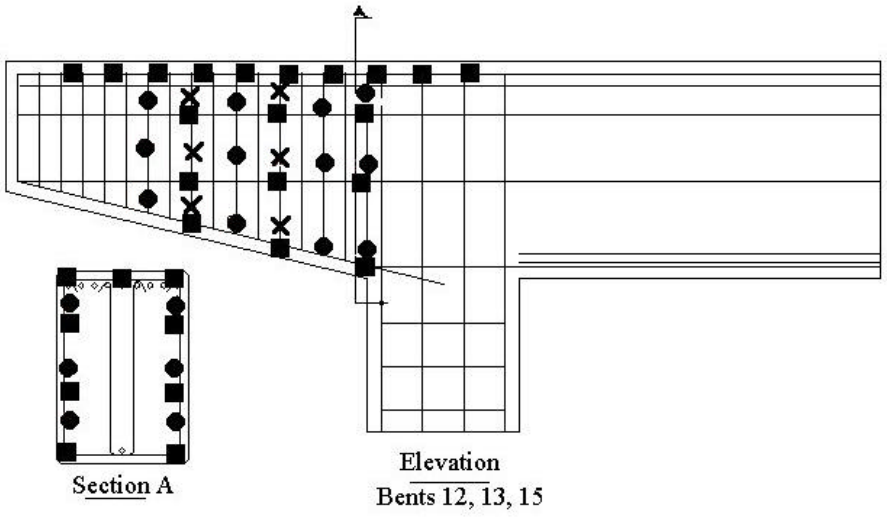


Figure 4.10 – Location of rebar strain gauges.

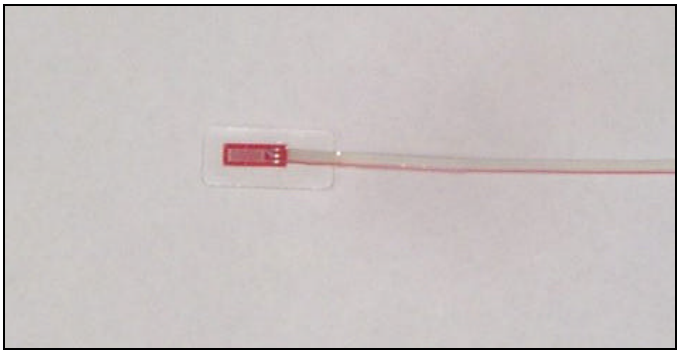

Figure 4.11 – Strain gauge used on large diameter rebar.

Figure 4.12 – Mounted rebar strain gauge.

Figure 4.13 – Mounted strain gauge with waterproof covering trimmed.

Figure 4.14 – Strain gauge lead wire torn off.

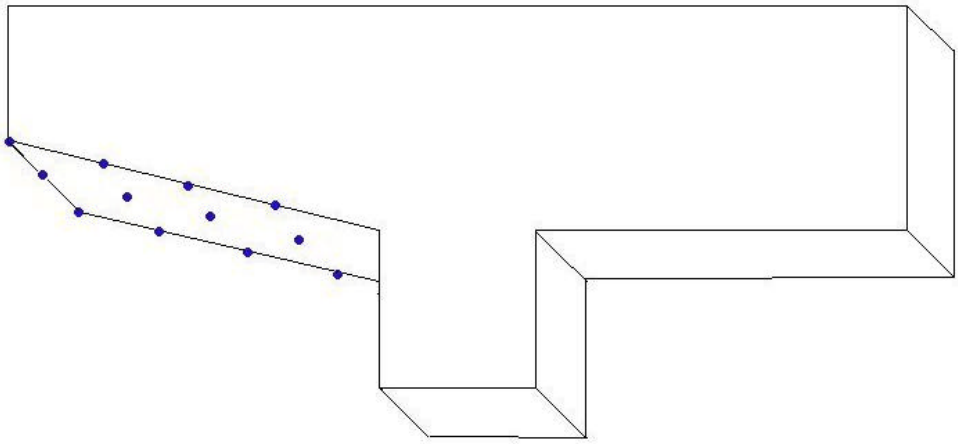

Figure 4.15 – Location of Deflection Measurements.

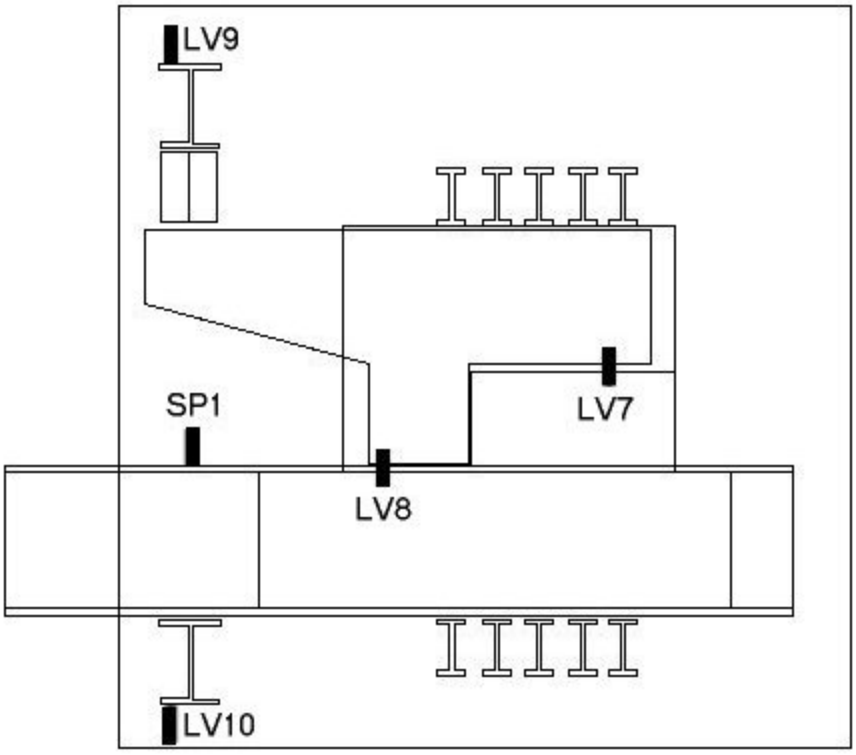


Figure 4.16 – Location of LVDT's on frame.

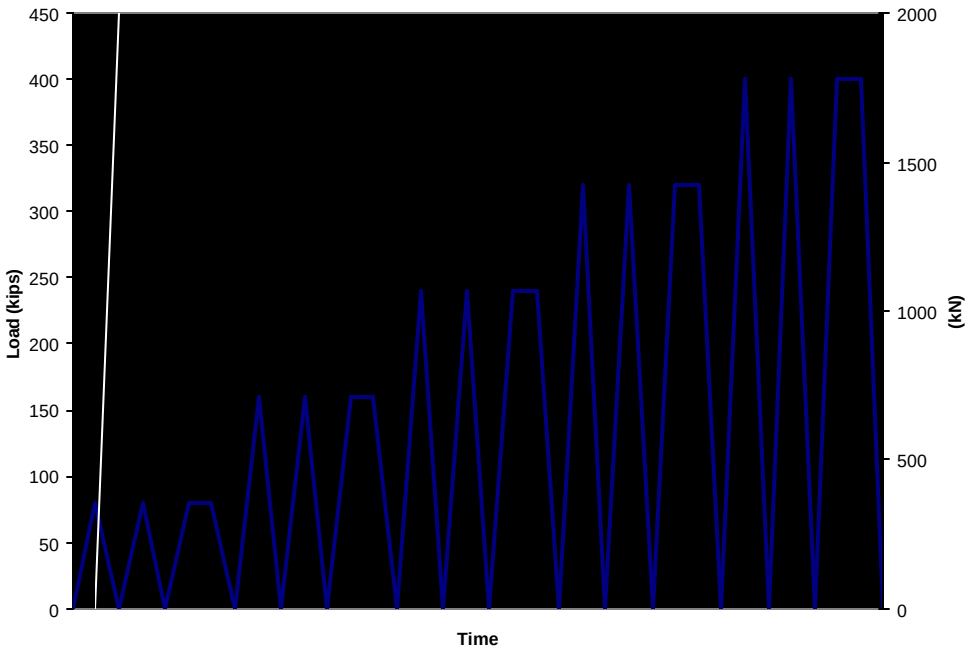


Fig. 4.17 – Loading Protocol for load controlled portion of all tests.

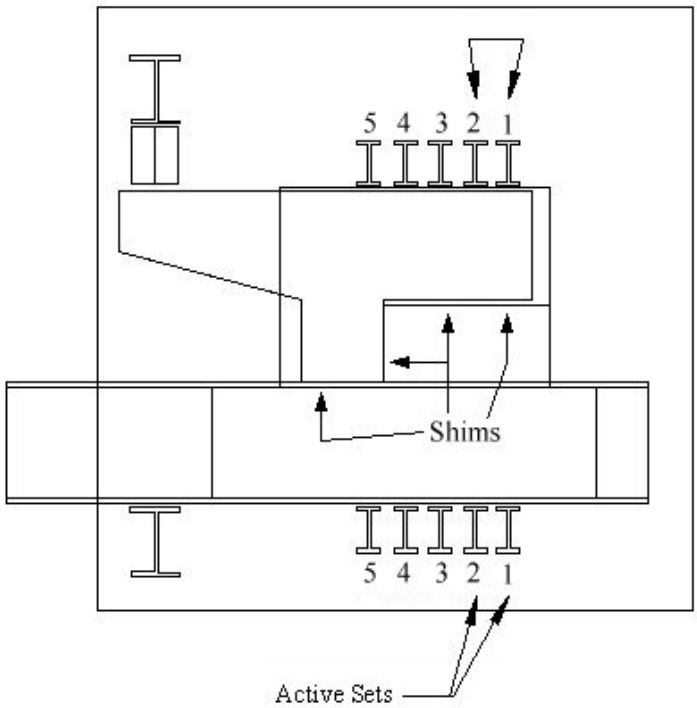


Figure 5.1 – Wood shims and active sets of shear beams in first test.

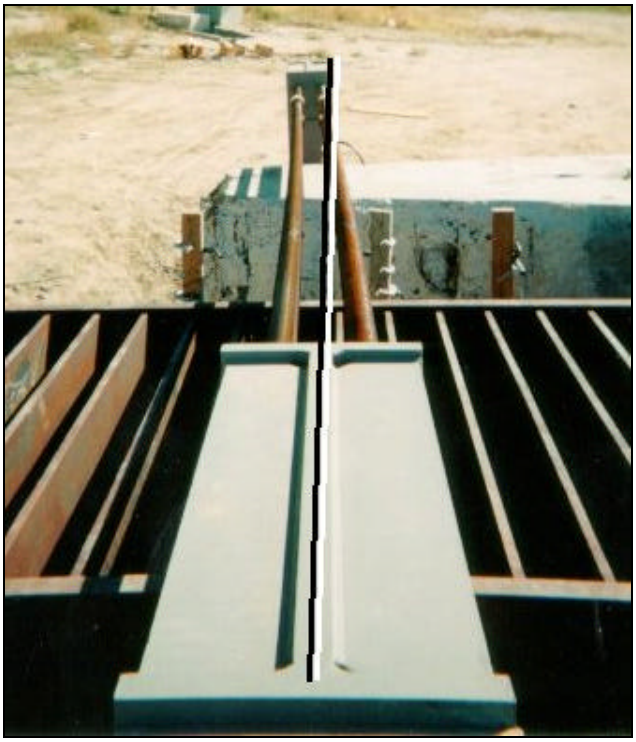

Figure 5.2 – Lateral movement of beam with actuators.

Figure 5.3 – Angles to prevent lateral movement of shear beam.

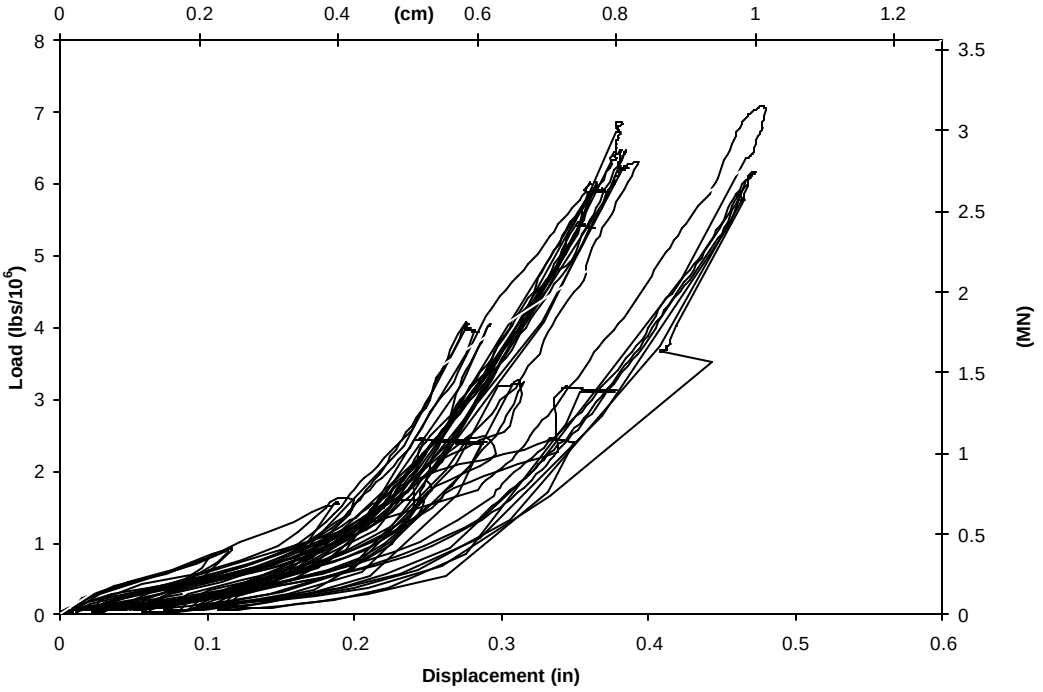


Figure 5.4 – LV7 during testing of bent 1N.

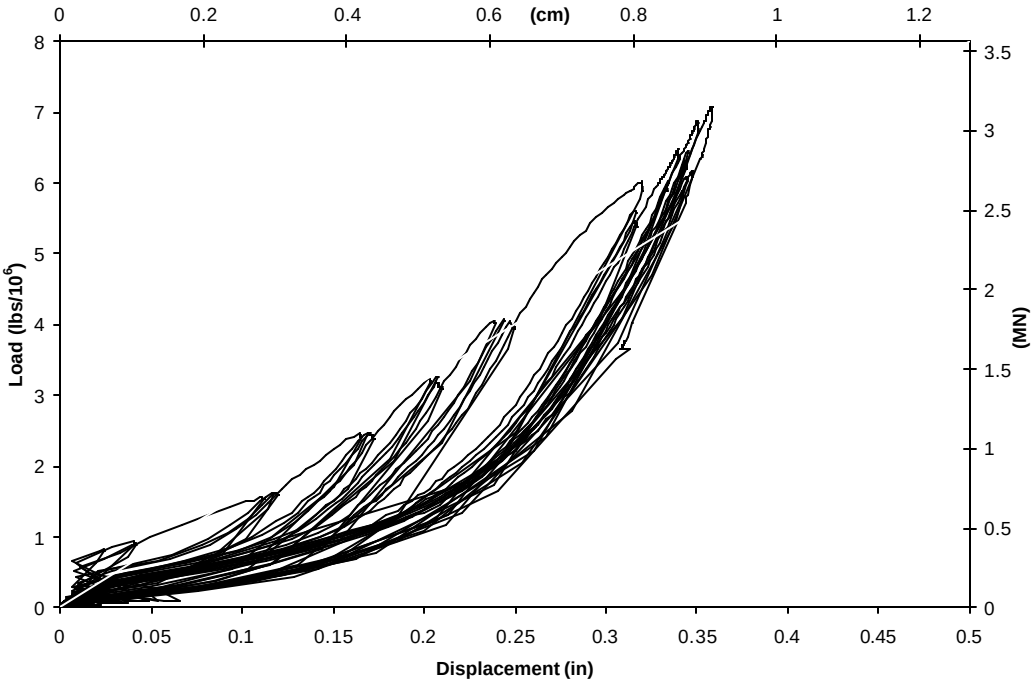


Figure 5.5 – LV8 during testing of bent 1N

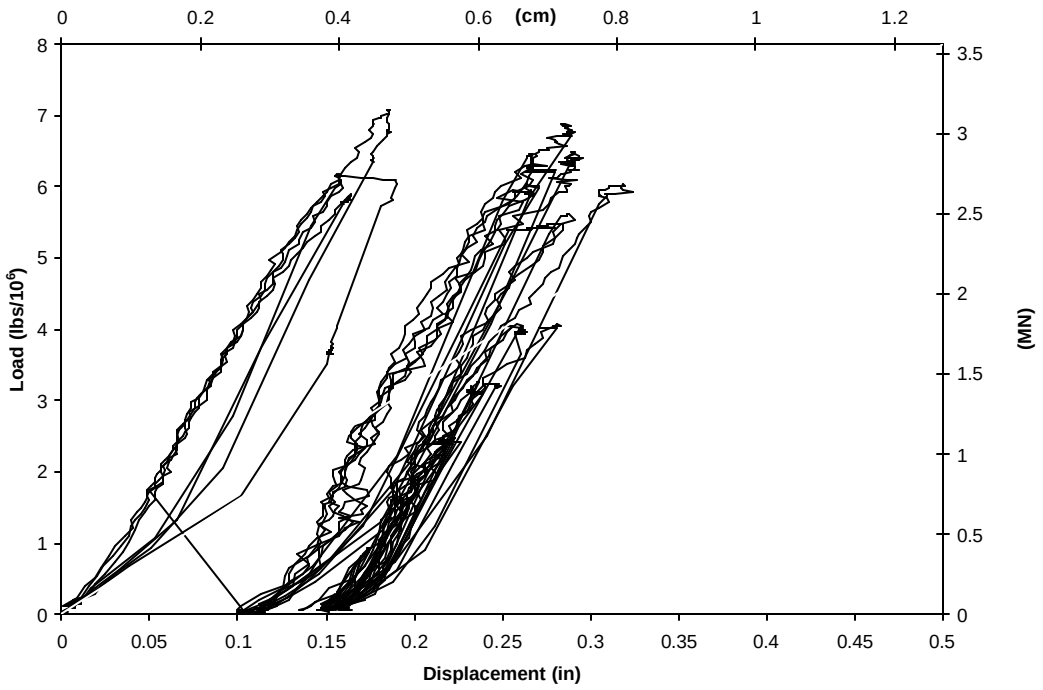


Figure 5.6 – SP1 during testing of bent 1N.


Figure 5.7 – Bent 12S, deterioration on underside of cantilever.

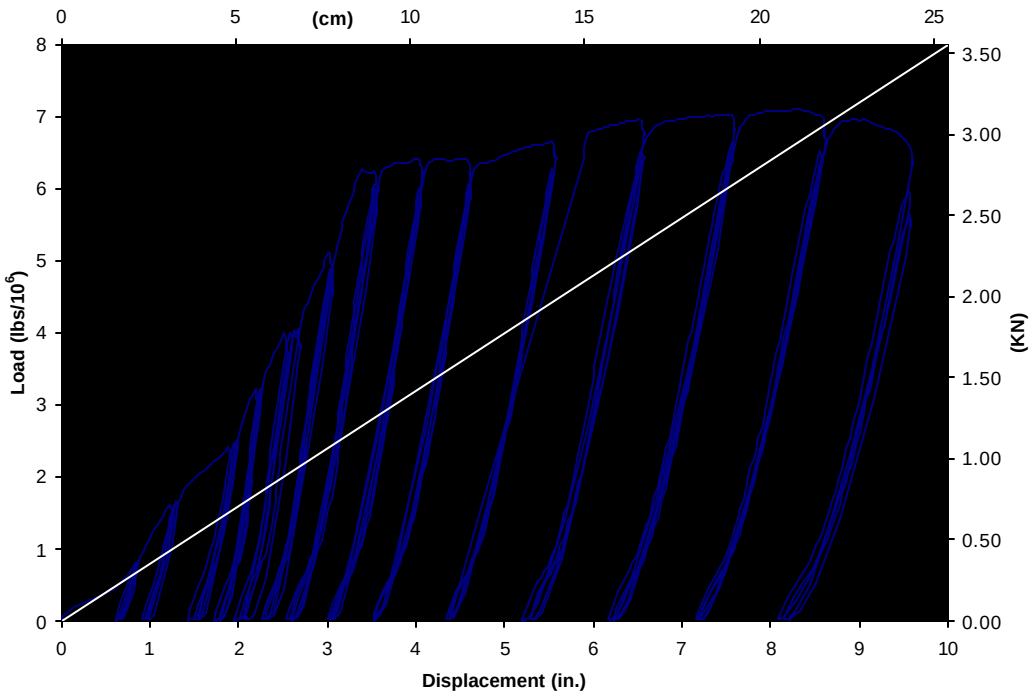


Figure 5.8 – Original load vs. tip displacement for bent 12S.

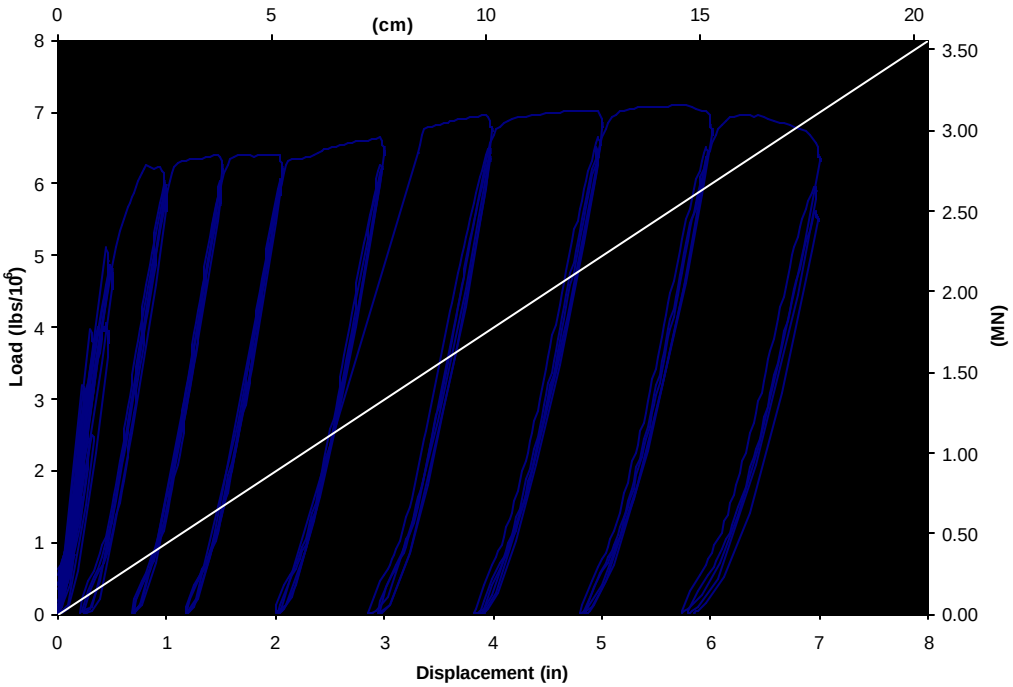


Figure 5.9 – Corrected load vs. tip displacement for bent 12S.

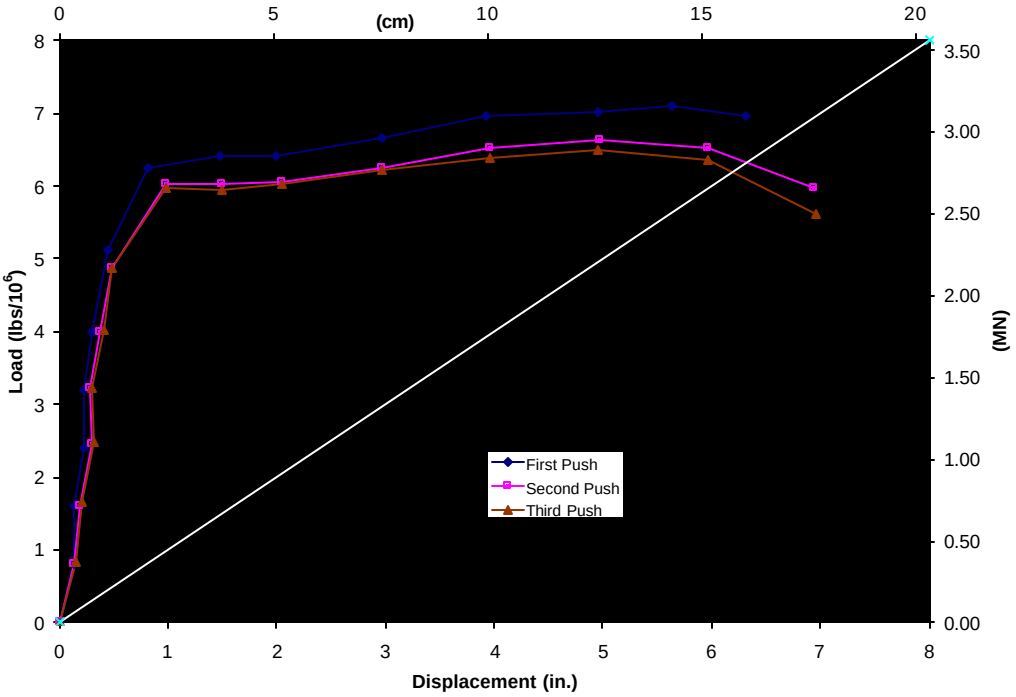


Figure 5.10 – Stiffness of each push for bent 12S.

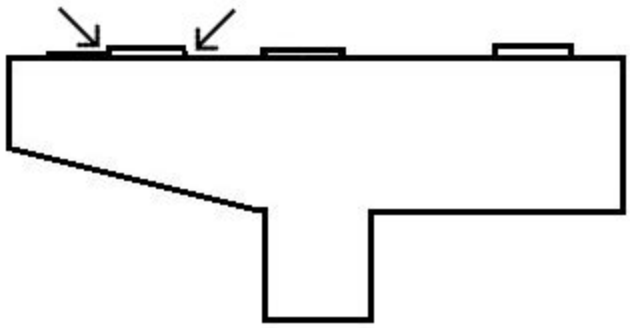

Figure 5.11 – Reentrant corners in girder pedestals and shear key.

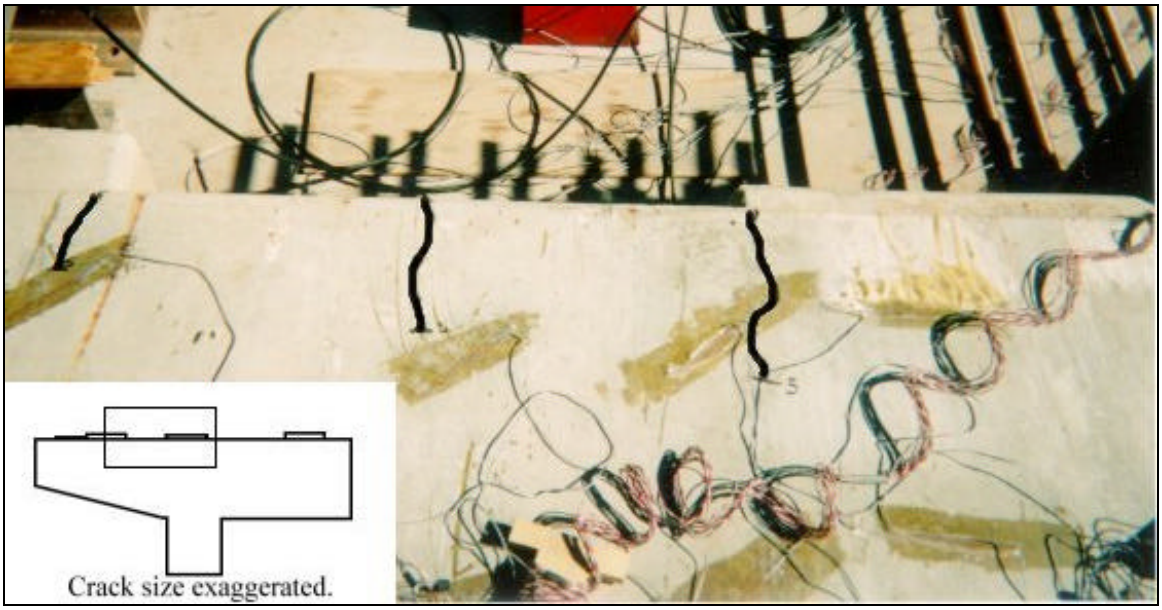


Figure 5.12 – Bent 12S, cracks on cycle 5.

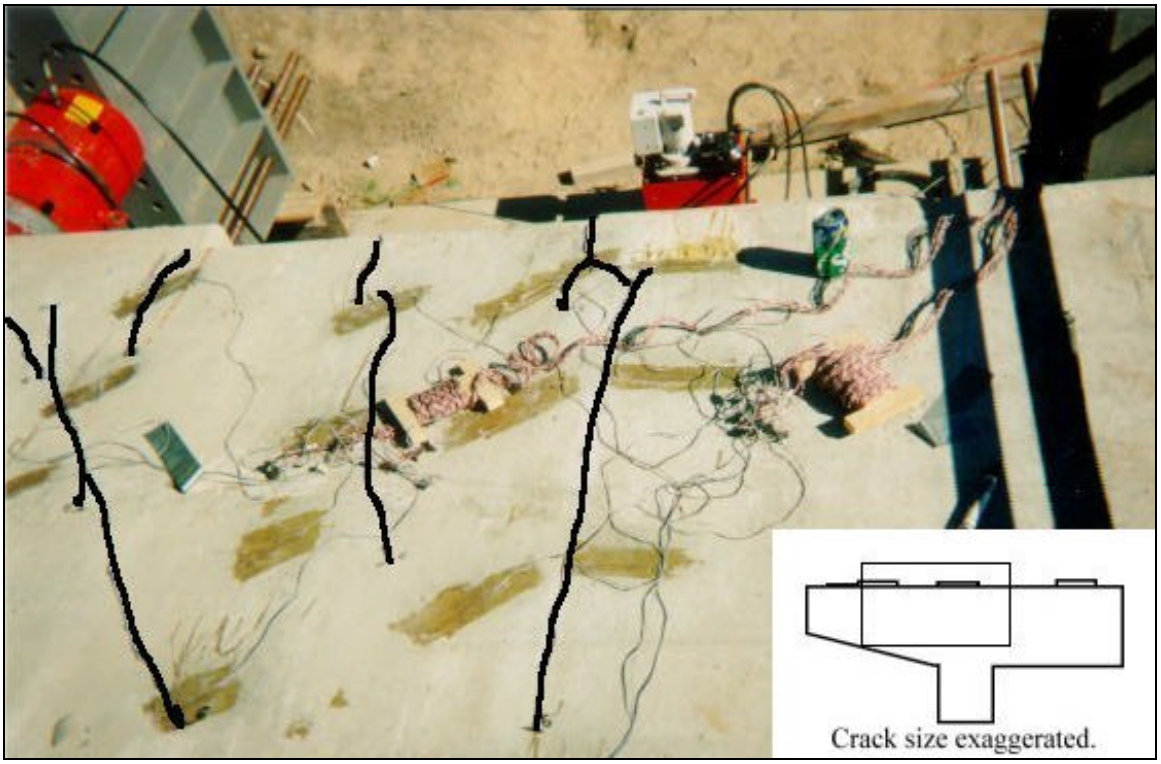


Figure 5.13 - Bent 12S, cracks on cycle 6.

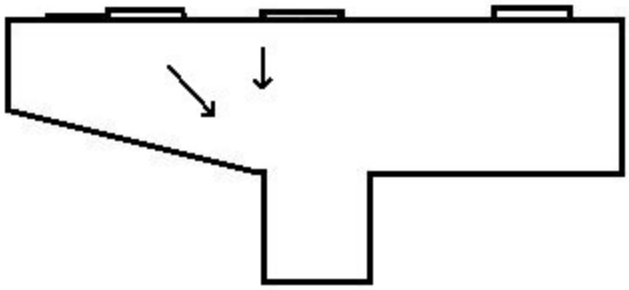

Figure 5.14 – Direction of propagation of cracks.

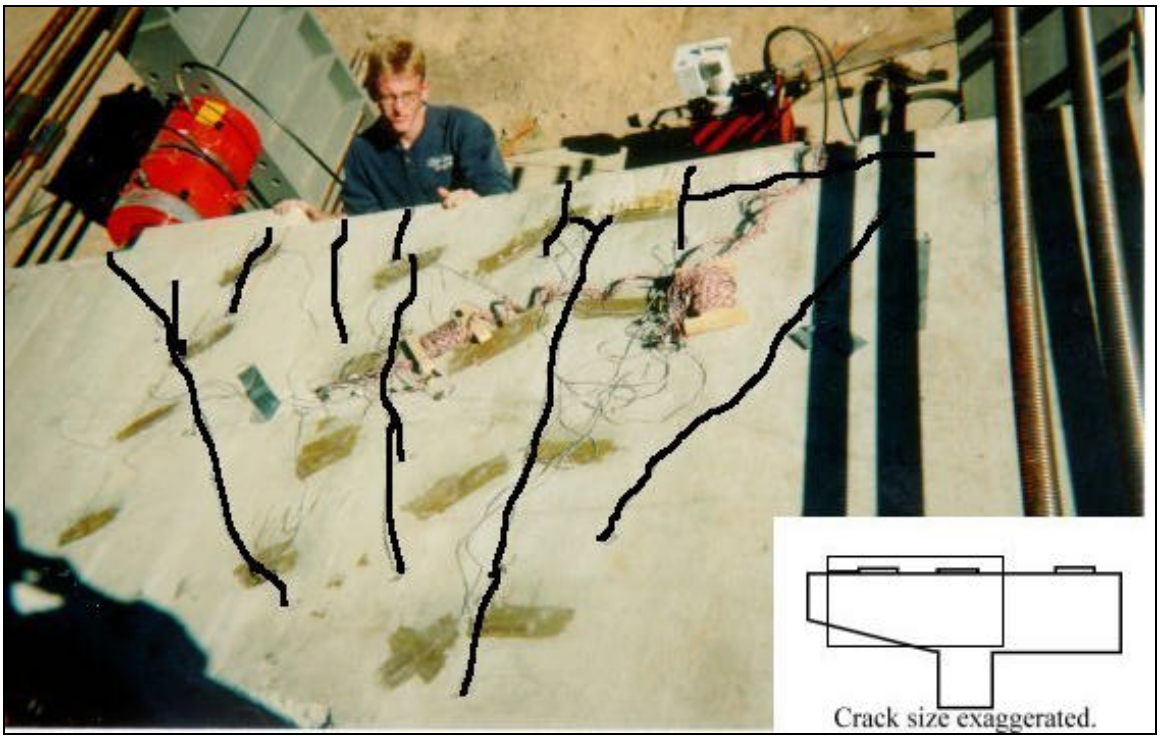


Figure 5.15 – Bent 12S, cracks on cycle 7.


Figure 5.16 – Bent 12S, cracks on cycle 8.

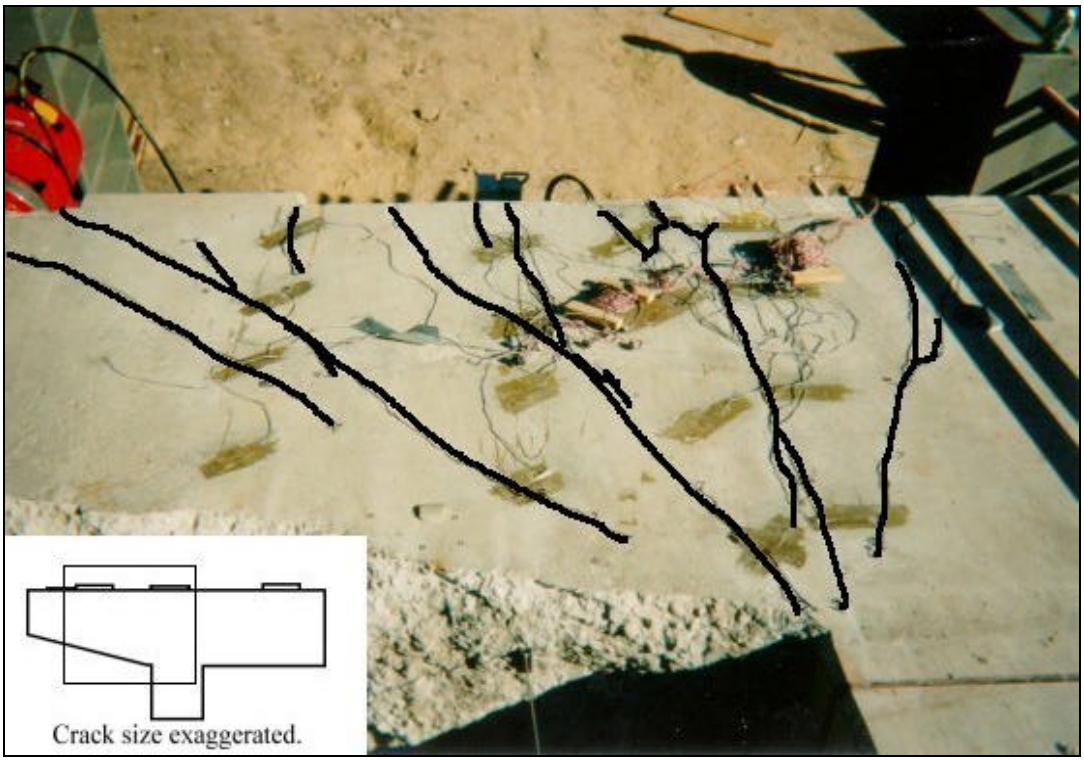


Figure 5.17 – Bent 12S, cracks on cycle 9.

Figure 5.18 – Bent 12S, crack in reentrant corner of pedestal and top of bent.


Figure 5.19 – Bent 12S, crack pattern at failure

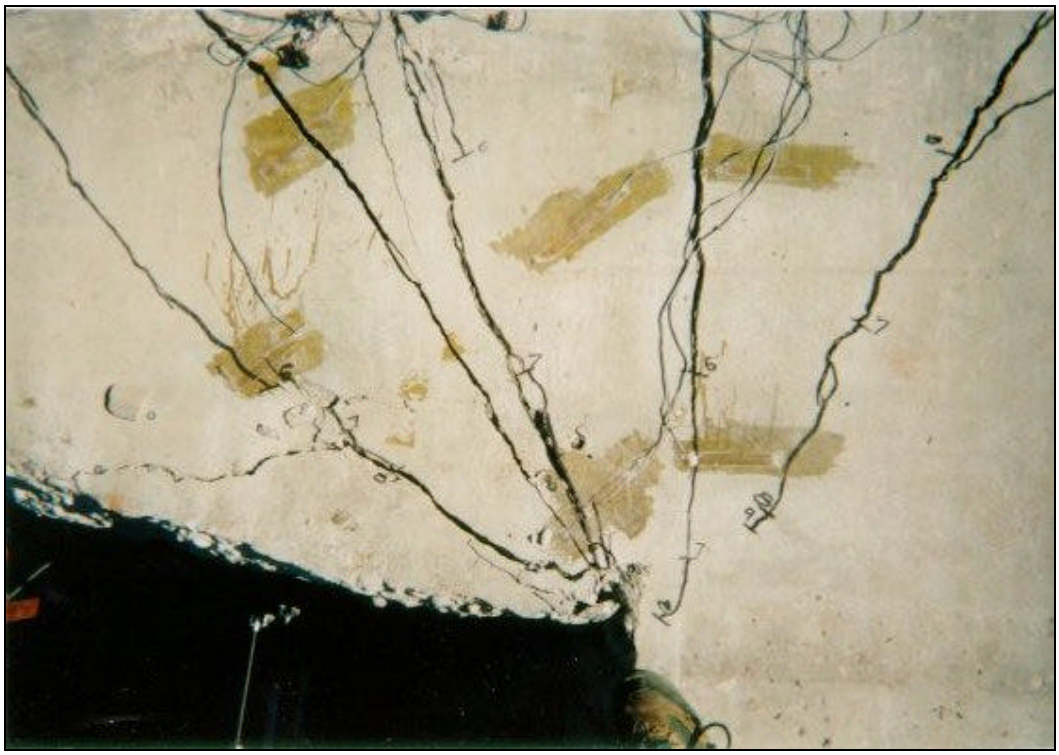

Figure 5.20 – Bent 12S, Compression zone after failure.


Figure 5.21 – Bent 12N, crack previous to testing, deterioration of underside of beam.

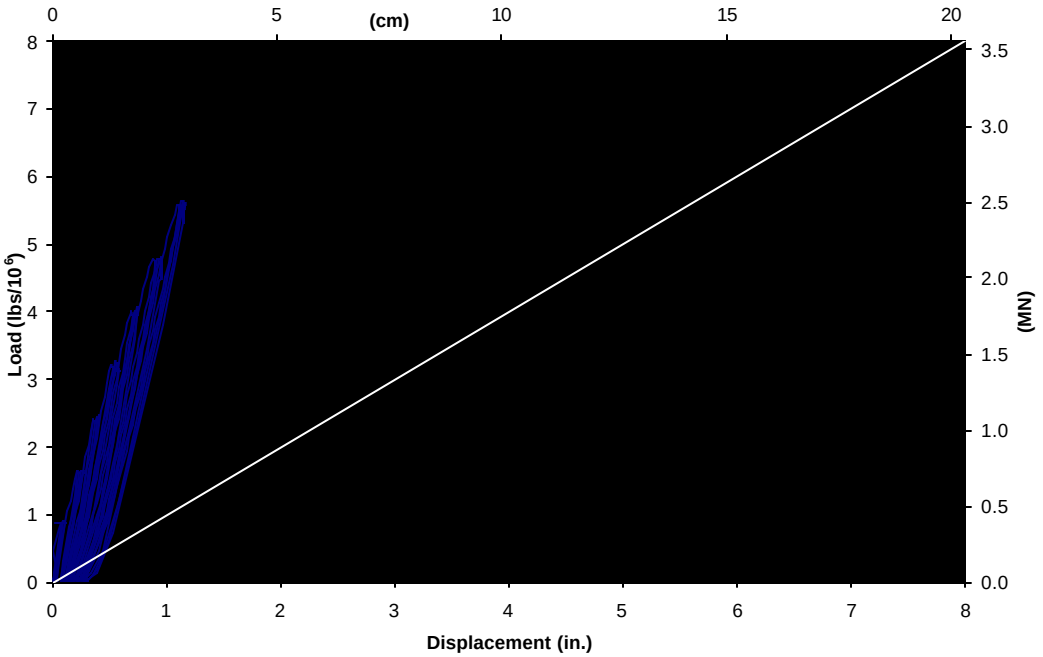


Figure 5.22 – Bent 12N, original load vs. displacement curve.

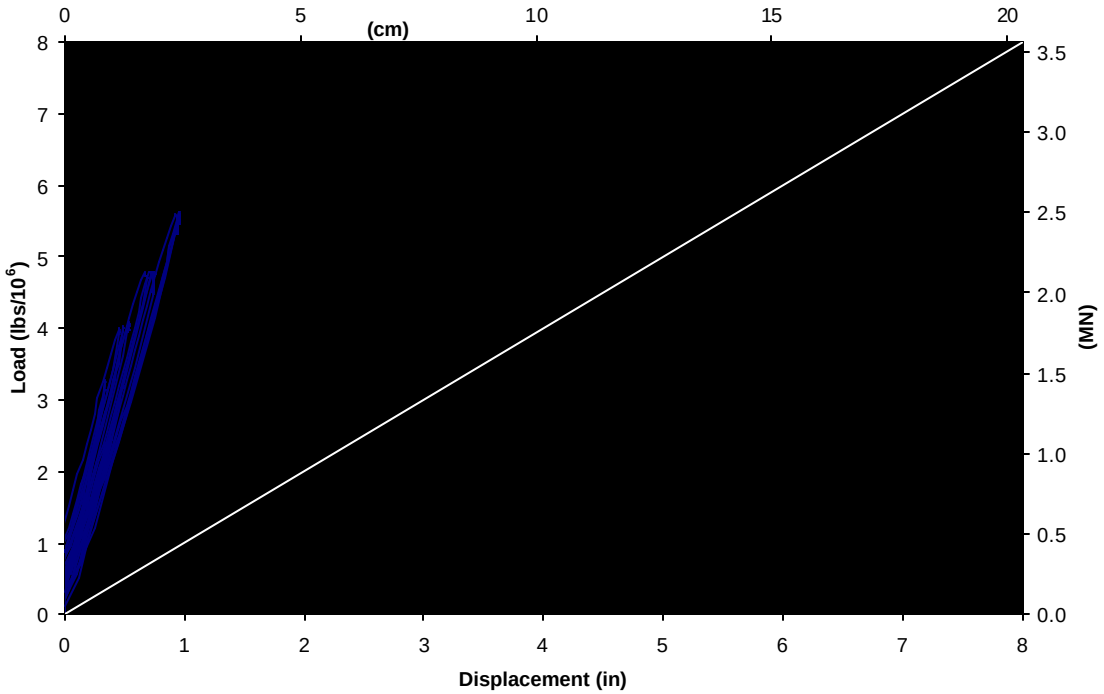


(a) – Overall Scale.

Figure 5.23 – Bent 12N, corrected load vs. displacement curve

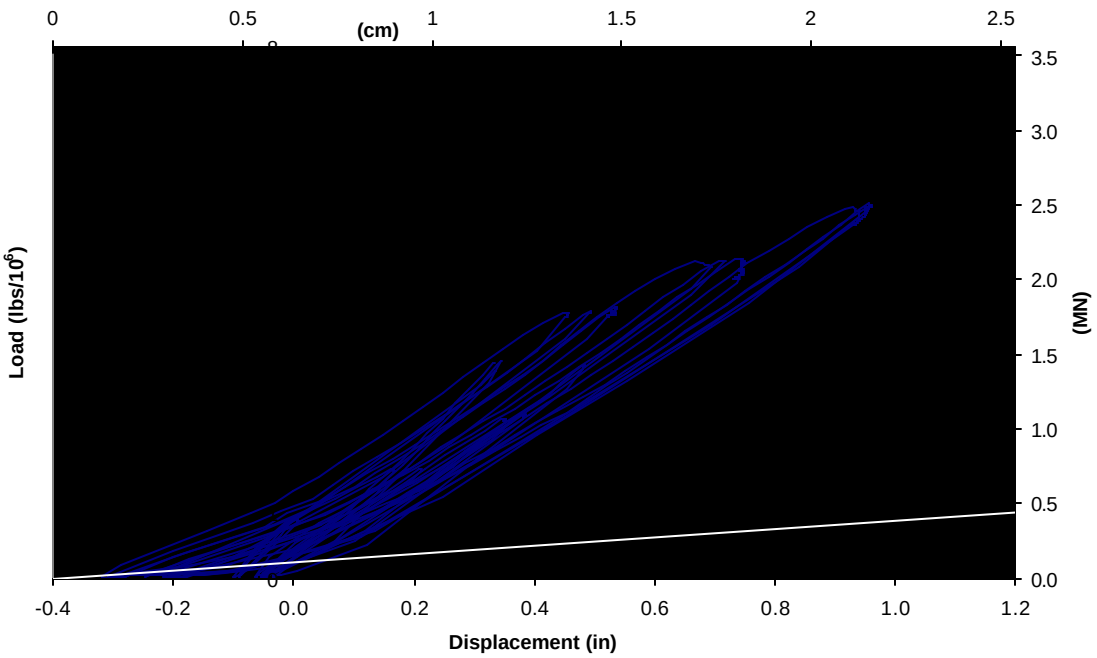


(b) – Compressed Scale.

Figure 5.23 (Cont.) – Bent 12N, corrected load vs. displacement curve.

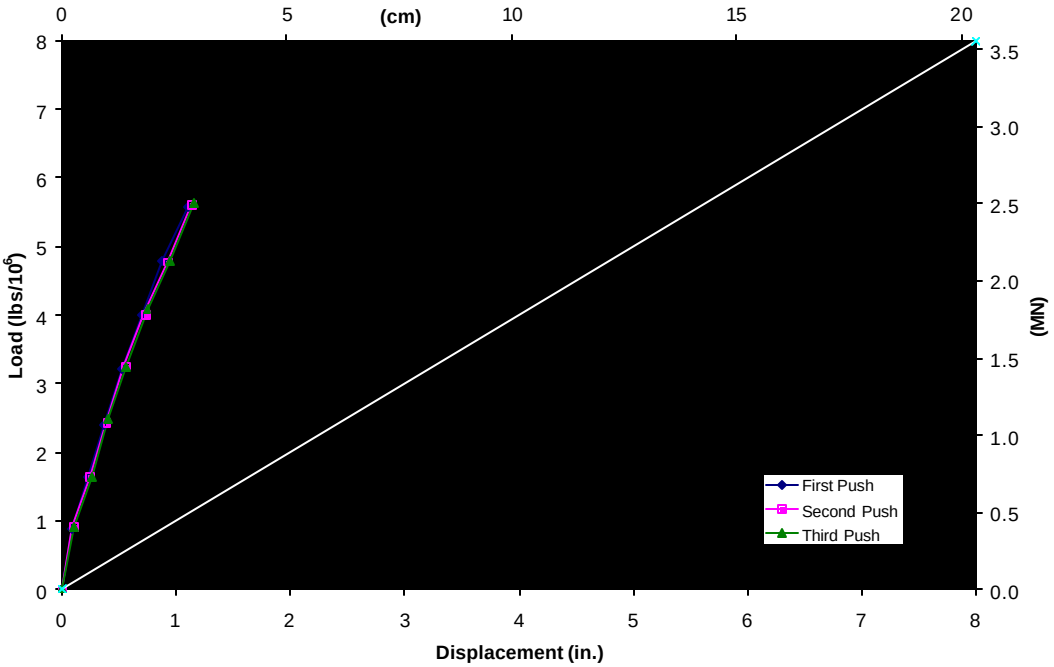


Figure 5.24 – Bent 12N, stiffness of each push.

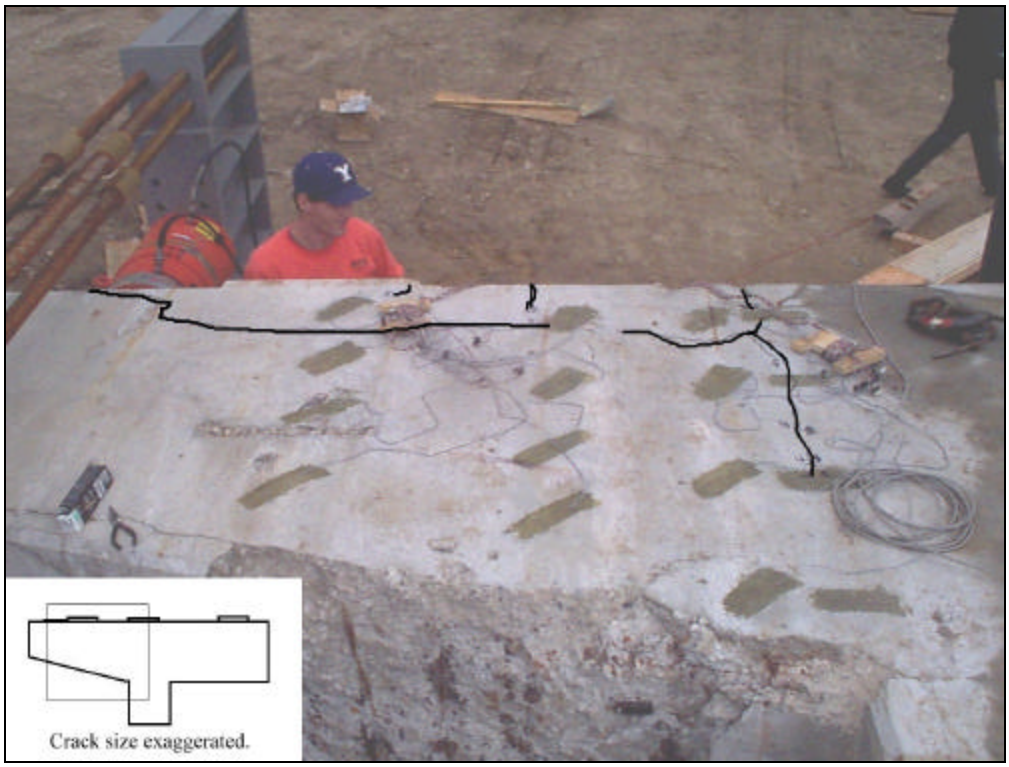


Figure 5.25 – Bent 12N, cracks on cycle 5.

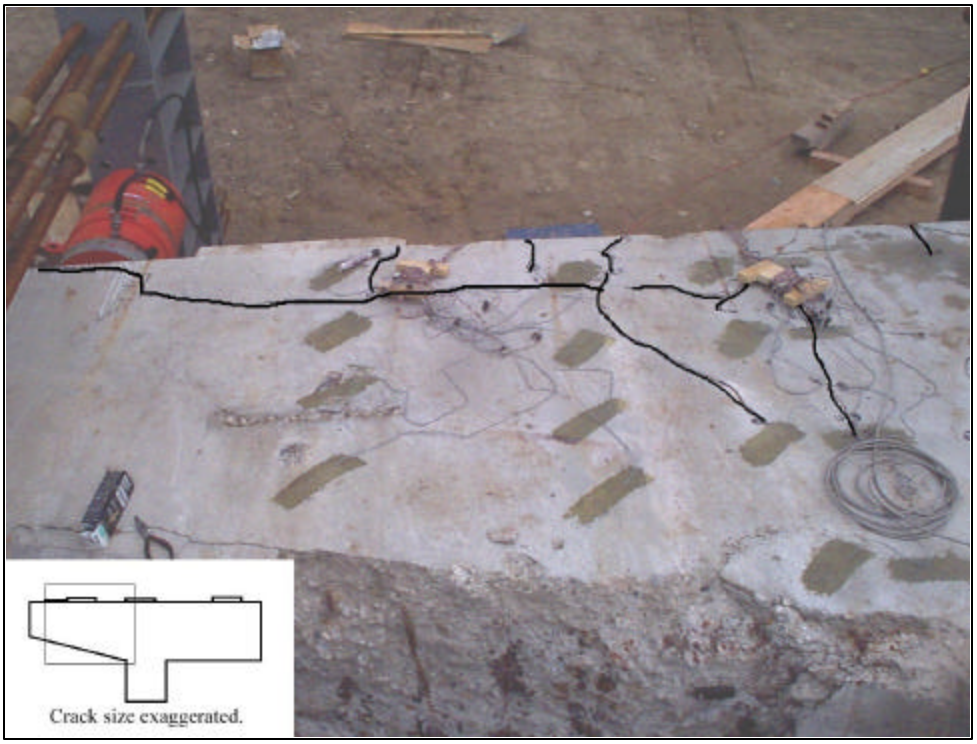


Figure 5.26 – Bent 12N, cracks on cycle 6.

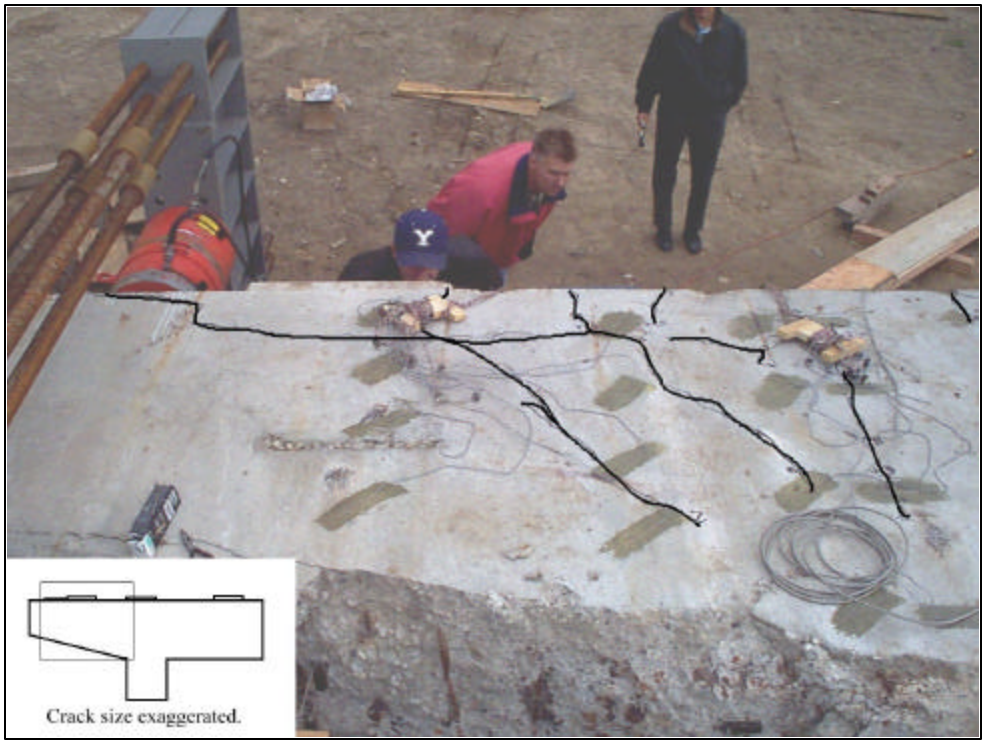


Figure 5.27 – Bent 12N, cracks on cycle 7.

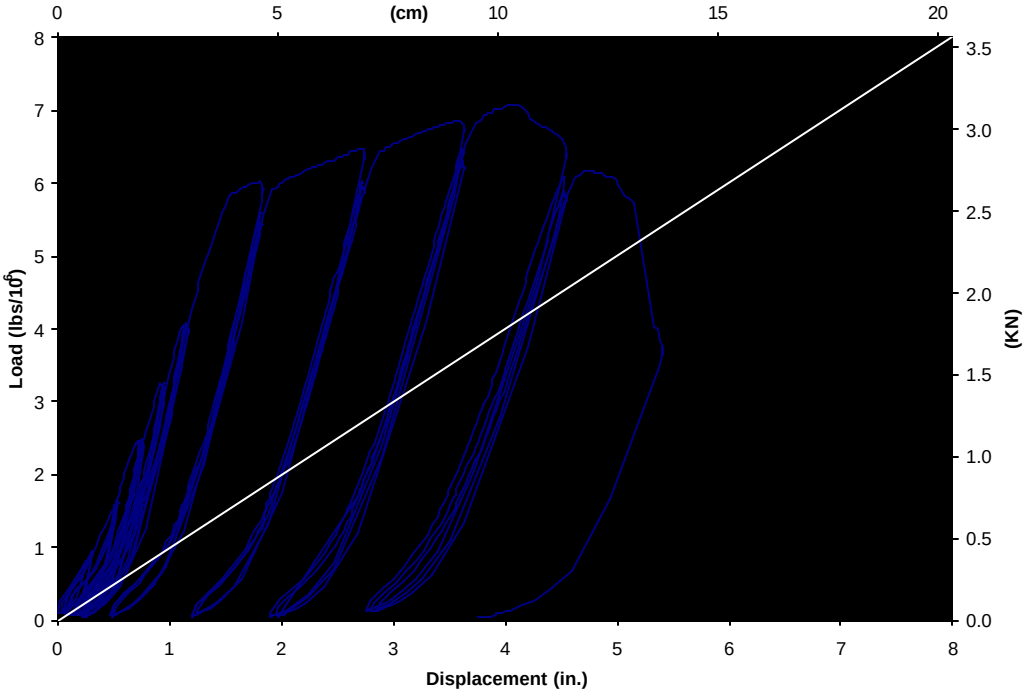


Figure 5.28 – Bent 1N, original load vs. displacement.

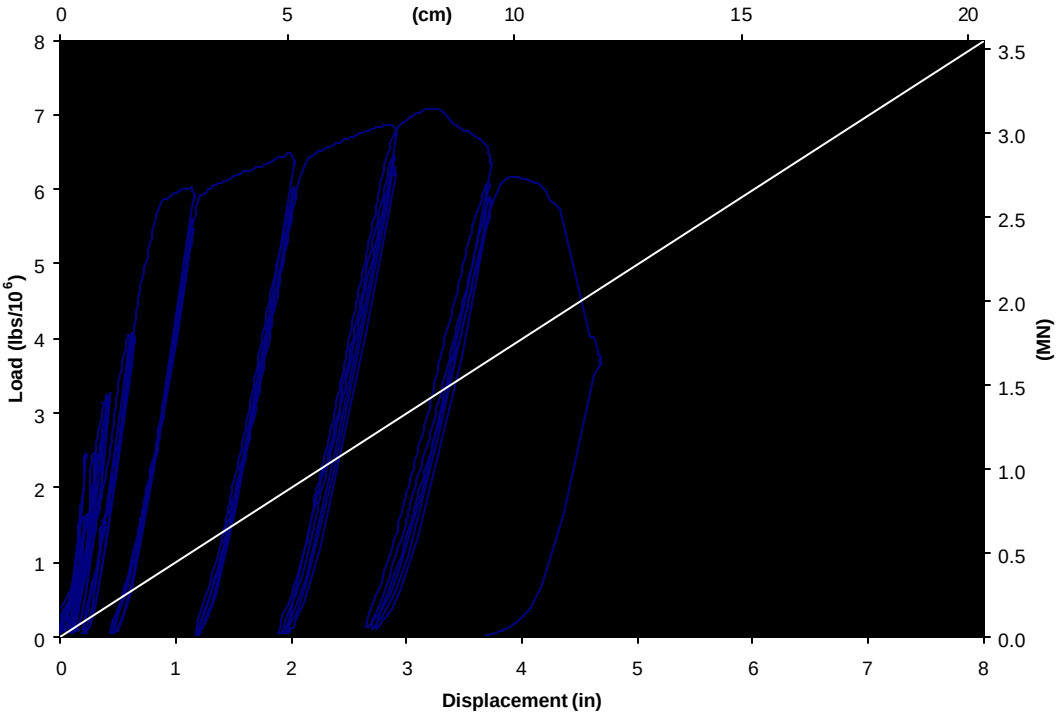


Figure 5.29 – Bent 1N, corrected load vs. displacement curve.

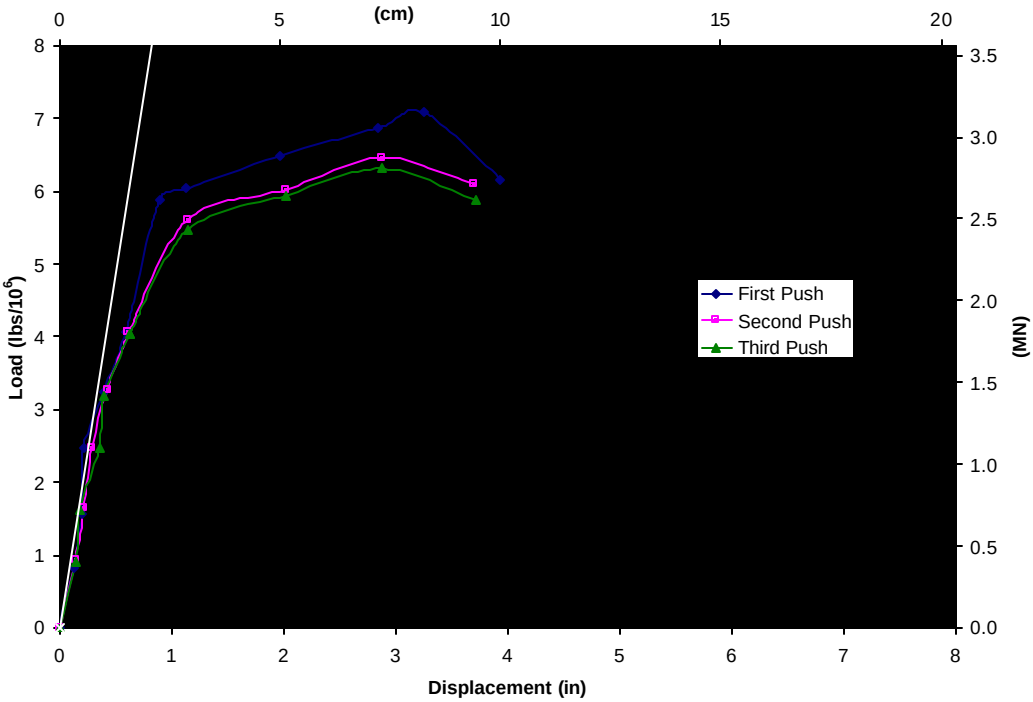


Figure 5.30 – Bent 1N, stiffness of each push.

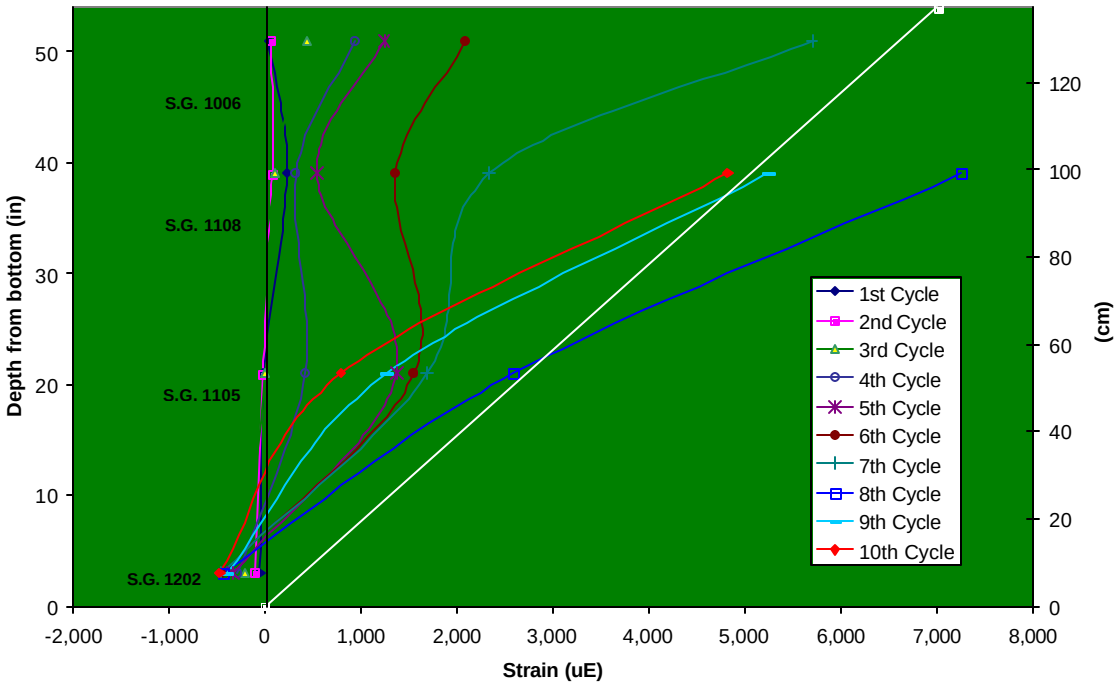


Figure 5.31 – Bent 1N, longitudinal strains on cross section.

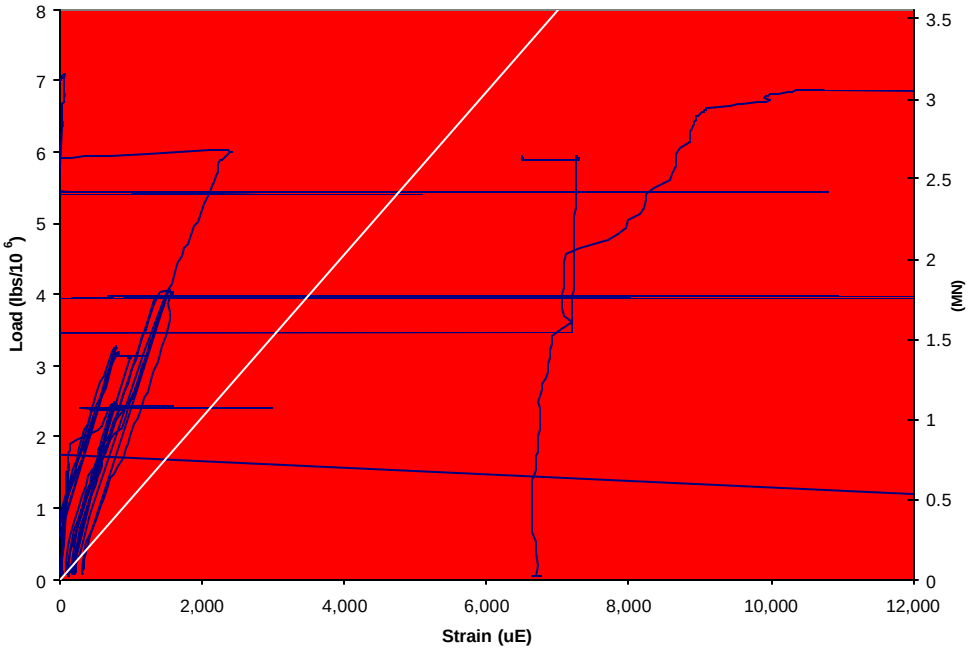


Figure 5.32 – Bent 1N, Strain on main flexural bar.

Figure 5.33 – Bent 1N, cracks on cycle 3.

Figure 5.34 – Bent 1N, cracks on cycle 4.

Figure 5.35 – Bent 1N, cracks on cycle 5.

Figure 5.36 – Bent 1N, cracks on cycle 6.

Figure 5.37 – Bent 1N, crushing of concrete.

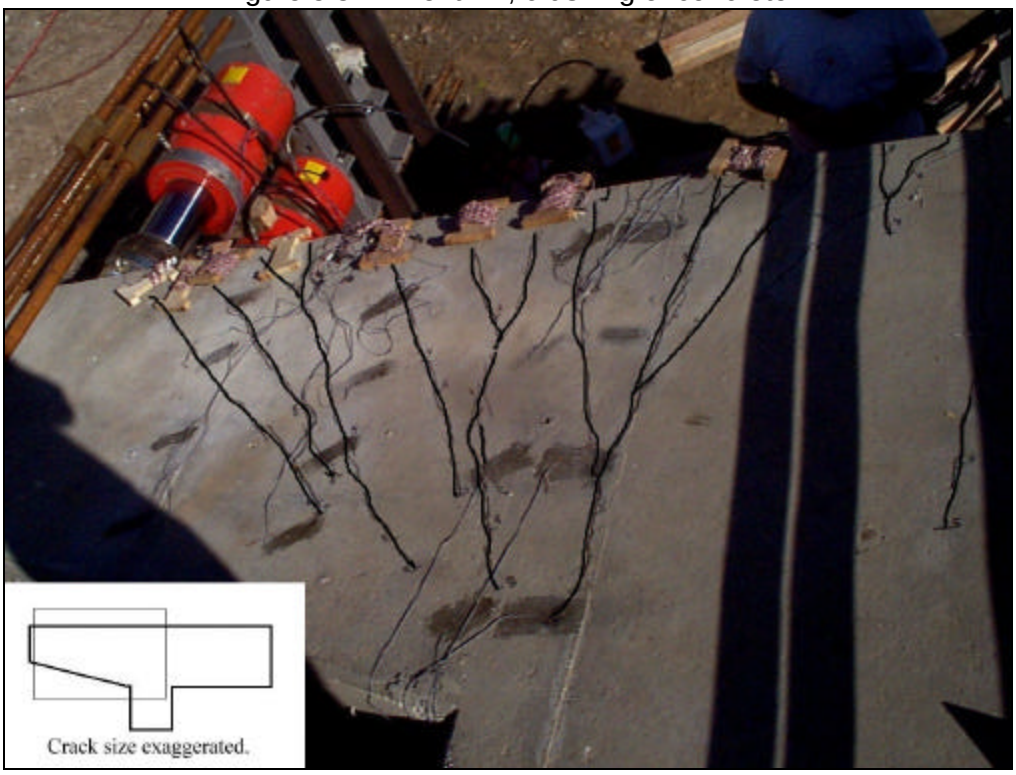


Figure 5.38 – Bent 1N, cracks on cycle 7.


Figure 5.39 – Bent 1N, cracks on cycle 8.

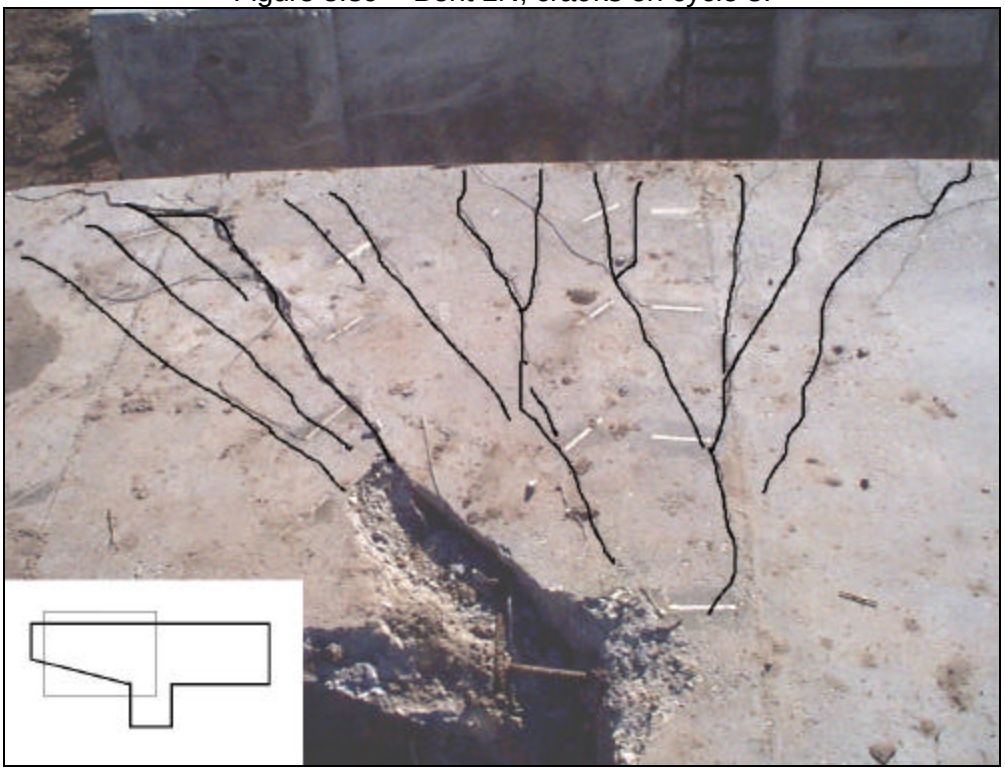

Figure 5.40 – Bent 1N, crack pattern at completion of test.

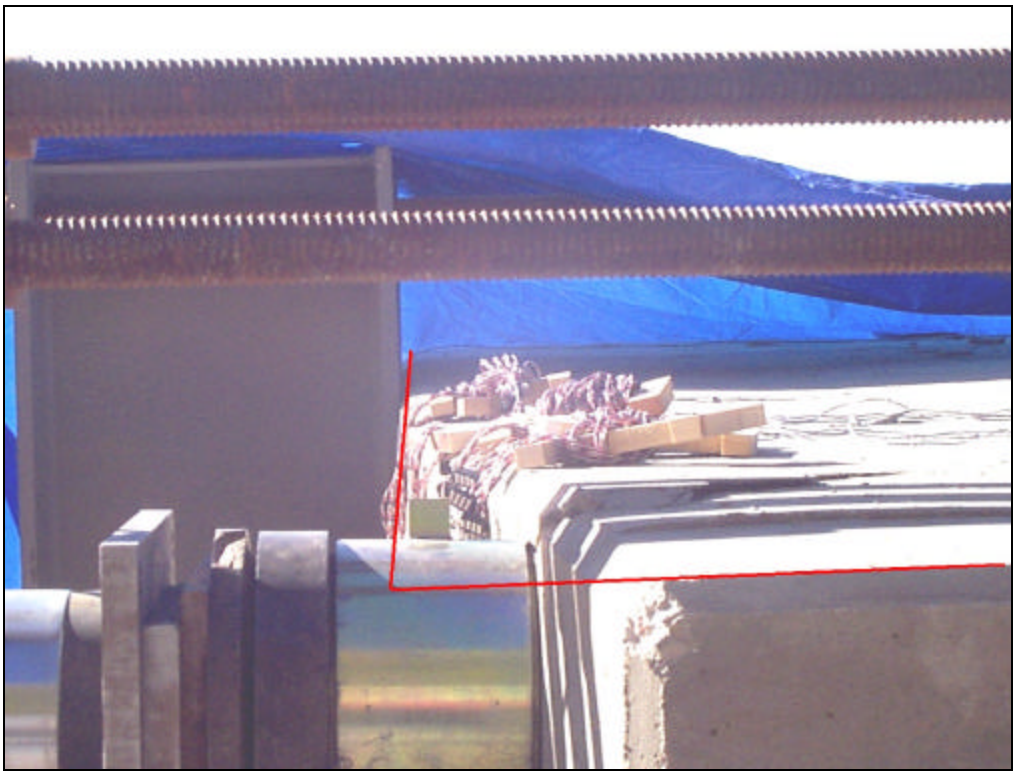

Figure 5.41– Permanent deflection at failure of bent 1N (line shows original position).

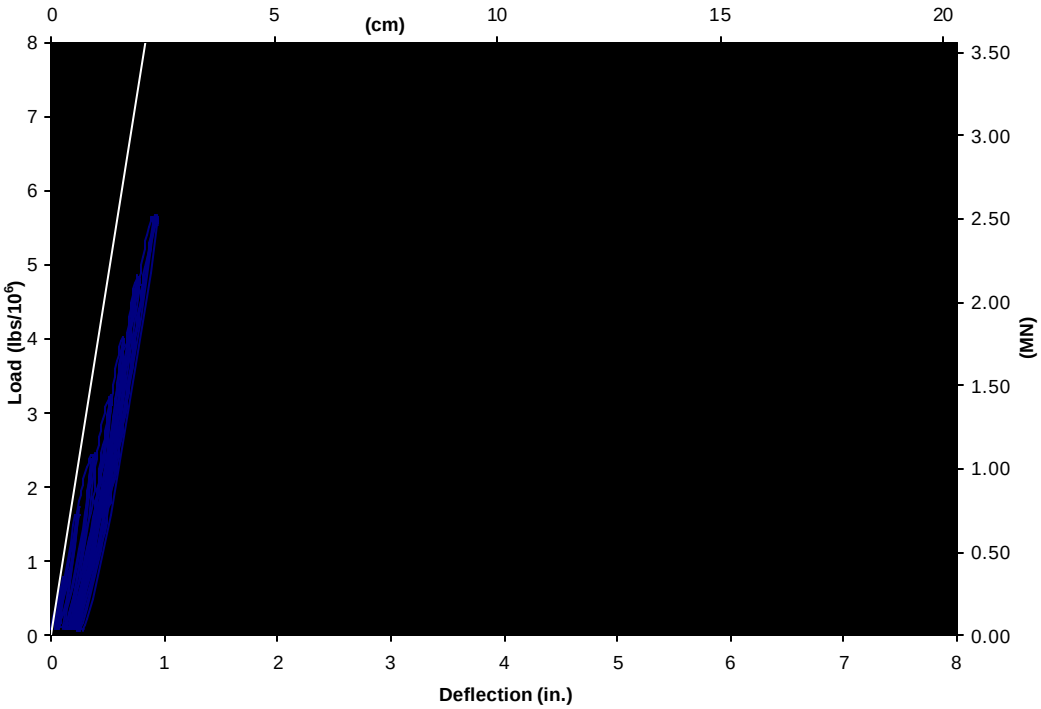


Figure 5.42 – Bent 2N, original load vs. displacement curve.

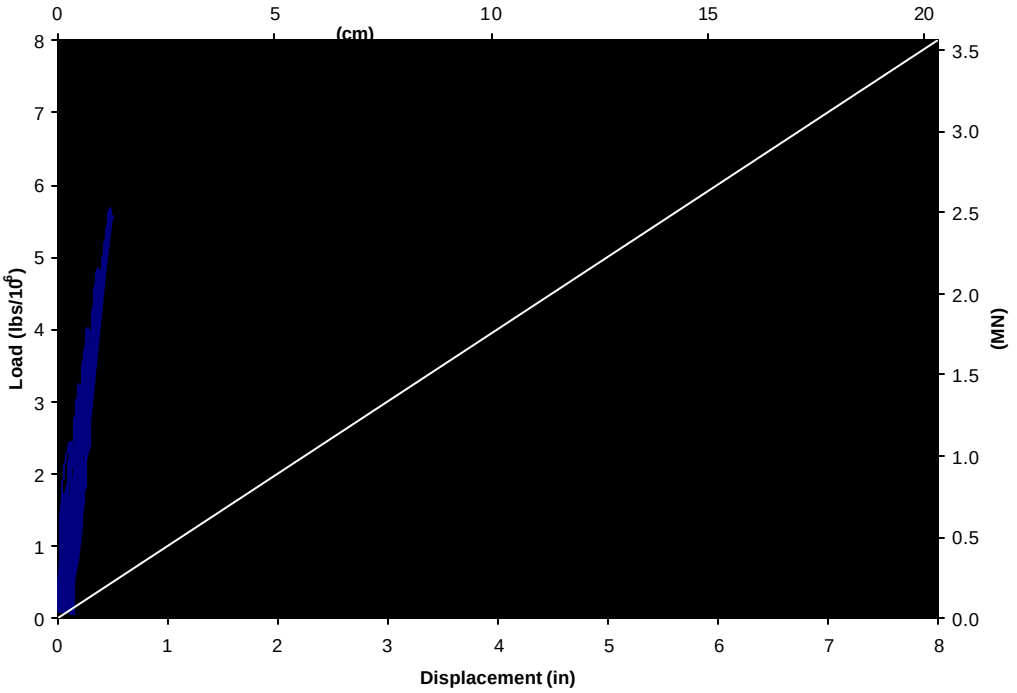


Figure 5.43 – Bent 2N, corrected load vs. displacement curve, overall scale

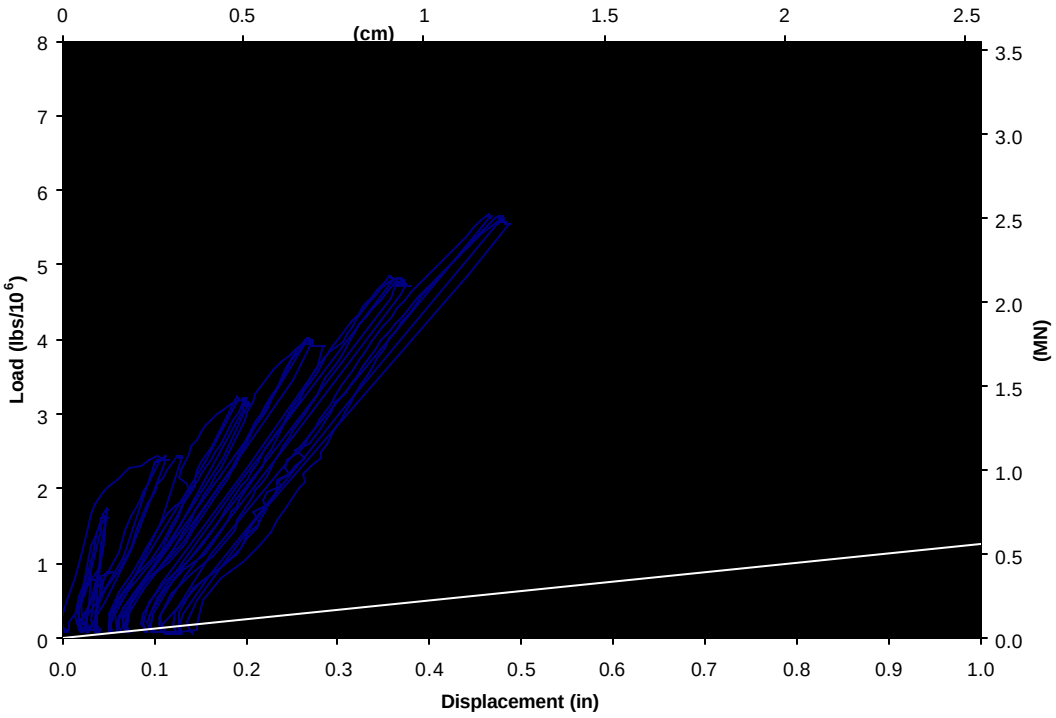


Figure 5.44 – Bent 2N, corrected load vs. displacement curve, compressed scale.

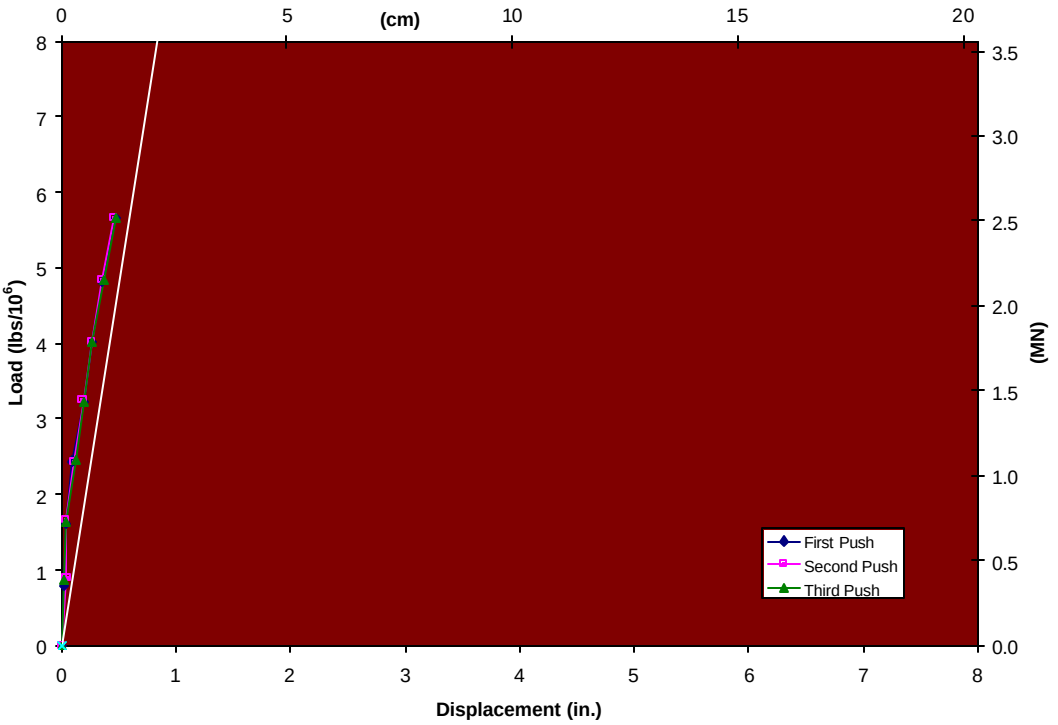


Figure 5.45 – Bent 2N, stiffness of each push.

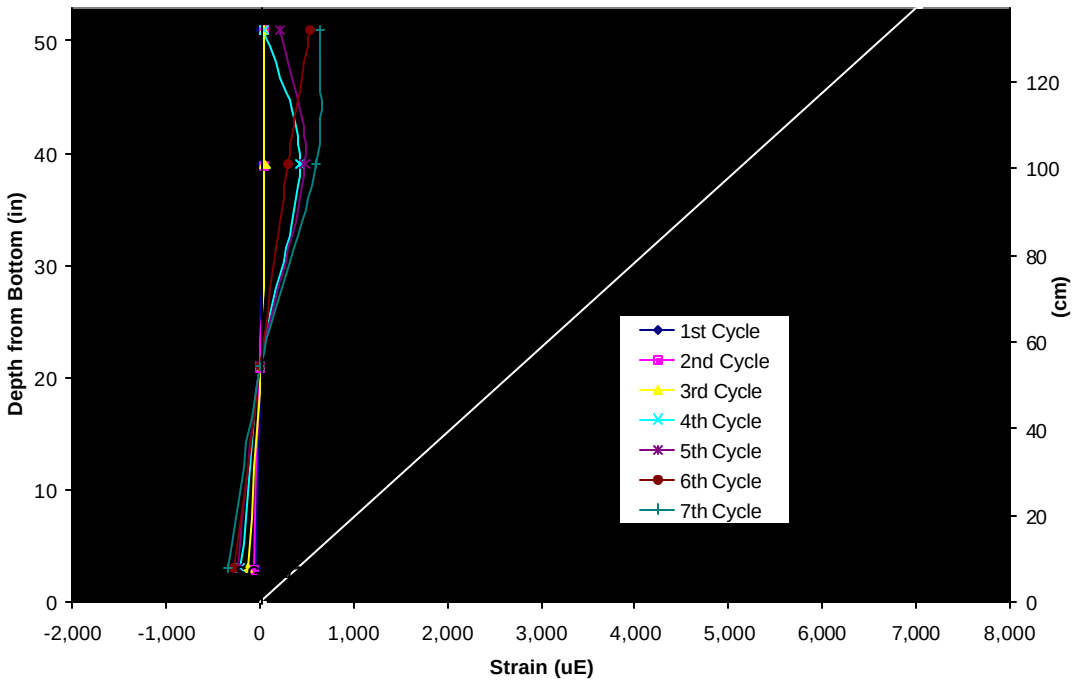


Figure 5.46 – Bent 2N, longitudinal strain.

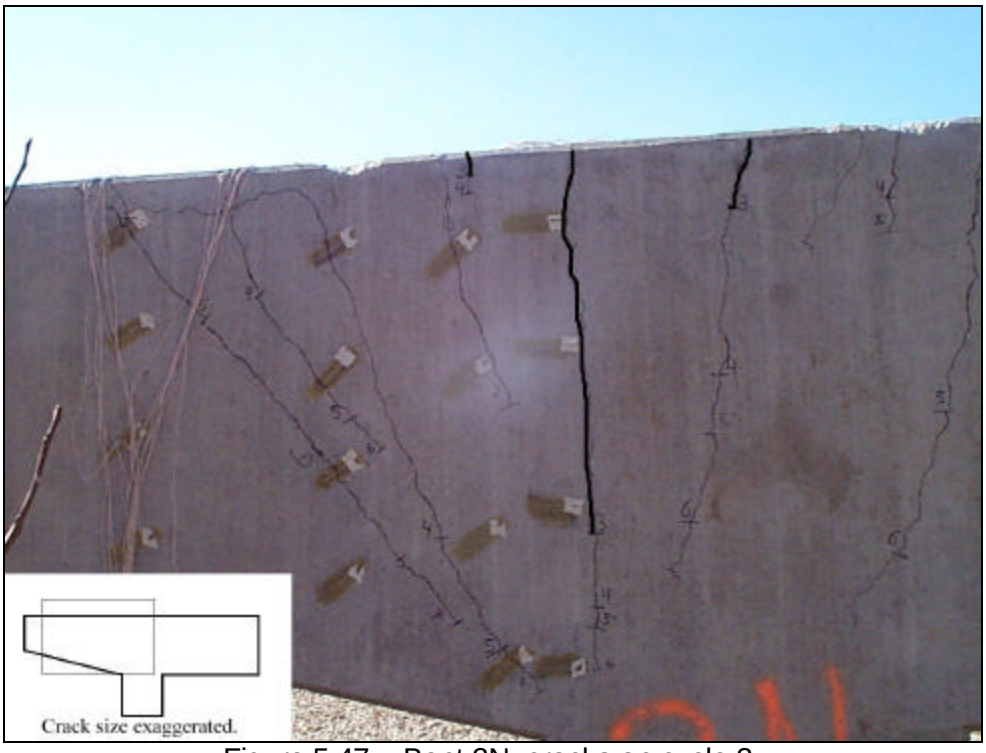


Figure 5.47 – Bent 2N, cracks on cycle 3.


Figure 5.48 – Bent 2N, cracks on cycle 4.


Figure 5.49 – Bent 2N, cracks on cycle 5.


Figure 5.50 – Bent 2N, cracks on cycle 6.


Figure 5.51 – Bent 2N, cracks on cycle 7.

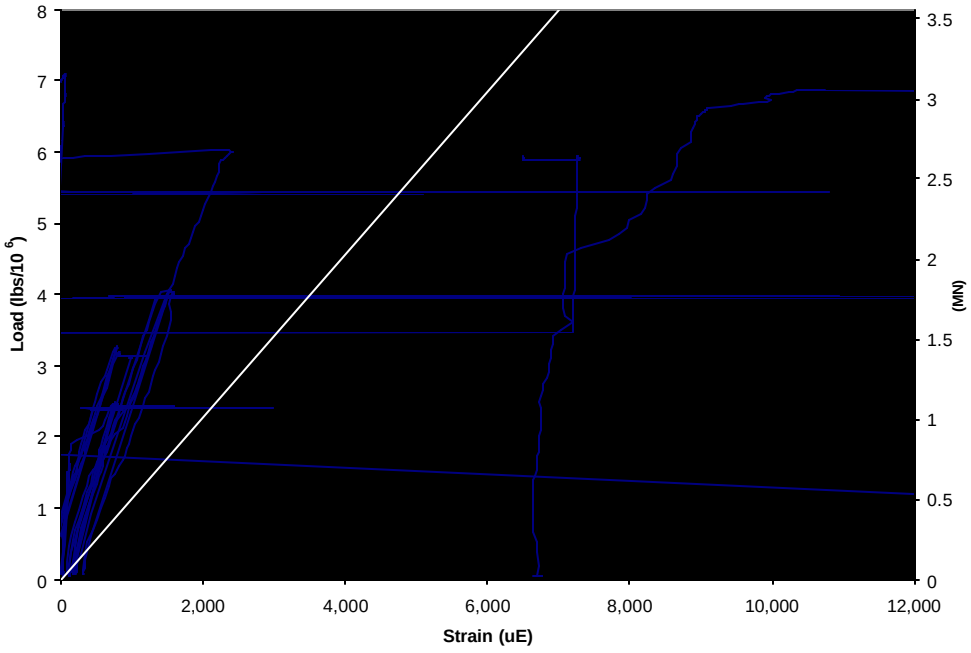


Figure 6.1 – Bent 1N, longitudinal strain of main flexural bar.

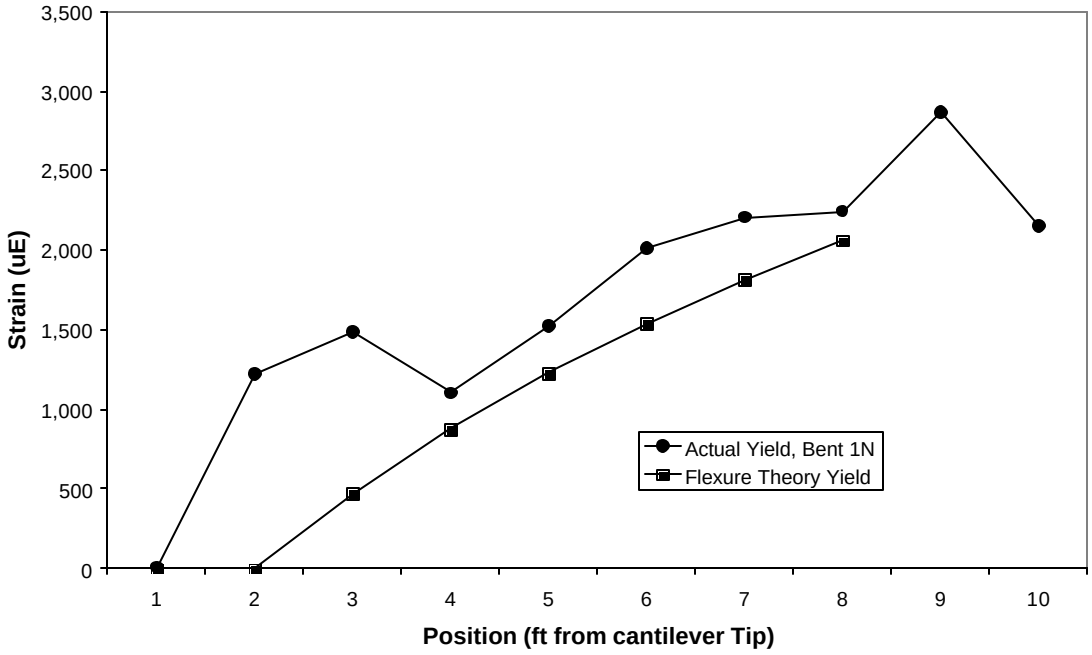


Figure 6.2 – Bent 1N, strain along length of main flexural bars compared to the strain predicted by Bernoulli beam theory

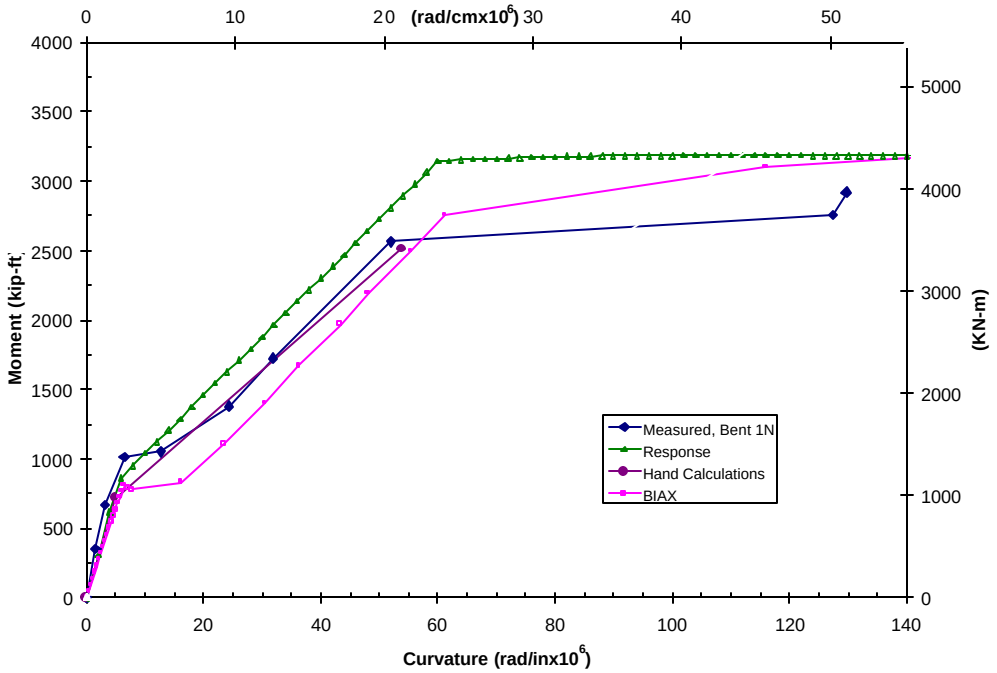


Figure 6.3 – Moment curvature

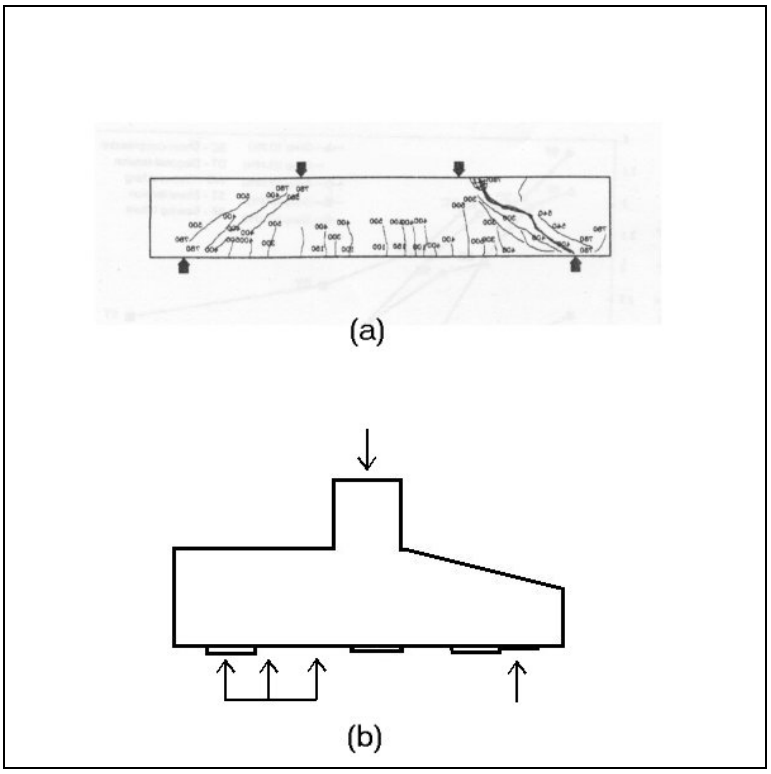

Figure 6.4 – (a) crack pattern from Tan, et al.. (b) loading of bents